Article
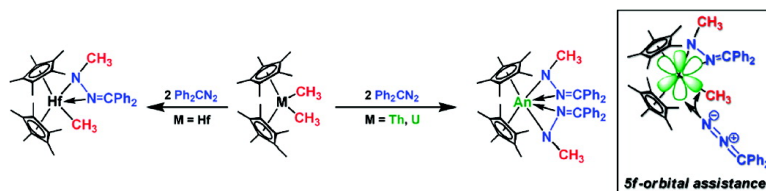
Evidence for the Involvement of 5f Orbitals in the Bonding and Reactivity of Organometallic Actinide Compounds: Thorium(IV) and Uranium(IV) Bis(hydrazonato) Complexes

Thibault Cantat, Christopher R. Graves, Kimberly C. Jantunen, Carol J. Burns, Brian L. Scott, Eric J. Schelter, David E. Morris, P. Jeffrey Hay, and Jaqueline L. Kiplinger

More About This Article

Additional resources and features associated with this article are available within the HTML version:

- Supporting Information
- Access to high resolution figures
- Links to articles and content related to this article
- Copyright permission to reproduce figures and/or text from this article

View the Full Text HTML

Evidence for the Involvement of 5f Orbitals in the Bonding and Reactivity of Organometallic Actinide Compounds: Thorium(IV) and Uranium(IV) Bis(hydrazonato) Complexes

Thibault Cantat, Christopher R. Graves, Kimberly C. Jantunen, Carol J. Burns,
Brian L. Scott, Eric J. Schelter, David E. Morris, P. Jeffrey Hay, and
Jaqueline L. Kiplinger*

Los Alamos National Laboratory, Los Alamos, New Mexico 87545

Received August 25, 2008; E-mail: kiplinger@lanl.gov

Abstract: Migratory insertion of diphenyldiazomethane into both metal−carbon bonds of the bis(alkyl) and bis(aryl) complexes $(C_5Me_5)_2AnR_2$ yields the first f-element bis(hydrazonato) complexes $(C_5Me_5)_2An[\eta^2$-(N,N')-R−N−N=$CPh_2]_2$ [An = Th, R = CH_3 (**18**), $PhCH_2$ (**15**), Ph (**16**); An = U, R = CH_3 (**17**), $PhCH_2$ (**14**)], which have been characterized by a combination of spectroscopy, electrochemistry, and X-ray crystallography. The two hydrazonato ligands adopt an η^2-coordination mode leading to 20-electron (for Th) and 22-electron (for U) complexes that have no transition-metal analogues. In fact, reaction of $(C_5H_5)_2Zr(CH_3)_2$ or $(C_5Me_5)_2Hf(CH_3)_2$ with diphenyldiazomethane is limited to the formation of the corresponding mono(hydrazonato) complex $(C_5R_5)_2M[\eta^2$-(N,N')-CH_3−N−N=$CPh_2](CH_3)$ (M = Zr, R = H or M = Hf, R = CH_3). The difference in the reactivities of the group 4 metal complexes and the actinides was used as a unique platform for investigating in depth the role of 5f orbitals on the reactivity and bonding in actinide organometallic complexes. The electronic structure of the $(C_5H_5)_2M[\eta^2$-(N,N')-CH_3−N−N=$CH_2]_2$ (M = Zr, Th, U) model complexes was studied using density functional theory (DFT) calculations and compared to experimental structural, electrochemical, and spectroscopic results. Whereas transition-metal bis(cyclopentadienyl) complexes are known to stabilize three ligands in the metallocene girdle to form saturated $(C_5H_5)_2ML_3$ species, in a bis(hydrazonato) system, a fourth ligand is coordinated to the metal center to give $(C_5H_5)_2ML_4$. DFT calculations have shown that 5f orbitals in the actinide complexes play a crucial role in stabilizing this fourth ligand by stabilizing both the σ and π electrons of the two η^2-coordinated hydrazonato ligands. In contrast, the stabilization of the hydrazonato ligands was found to be significantly less effective for the putative bis(hydrazonato) zirconium(IV) complex, yielding a higher energy structure. However, the difference in the reactivities of the group 4 metal and actinide complexes does not arise on thermodynamic grounds but is primarily of kinetic origin. Unfavorable steric factors have been ruled out as the sole influence to explain these different behaviors, and electronic factors were shown to govern the reactivity. For the actinides, both the C_5H_5 and more realistic C_5Me_5 ligands have been taken into account in computing the energy surface. The reaction profile for the C_5Me_5 system differs from that with the C_5H_5 ligand by a uniform shift of ∼5 kcal/mol in the relative energies of the transition state and products. The insertion of a second diazoalkane molecule into the sole metal−carbon bond in the mono(hydrazonato) complexes involves a high energy barrier (∼20 kcal/mol) for the zirconium(IV) system, whereas the actinides can facilitate the approach of the diazoalkane by coordination (formation of an adduct) and its insertion into the An−C bond with a very low barrier on the potential energy surface.

Introduction

The role of the 5f orbitals in bonding and reactivity is still one of the most intriguing questions in actinide chemistry and continues to be a topic of considerable debate among theoretical and experimental chemists.[1,2] The high nodality of the 5f orbitals, coupled with the fact that many organoactinide complexes possess expanded electron counts,[3] provides the opportunity for the actinide metals to engage in bonding schemes and chemistries that are not available to the d-transition metals.[4−21] A vivid illustration of this behavior is provided by the four-electron reductive cleavage of the N=N double bond in azobenzene by $(C_5Me_5)_2UCl_2$ (**1**)/(Na/Hg),[22] $(C_5Me_5)_3U$ (**2**),[23] $[(C_5Me_5)_2U][(\mu$-Ph$)_2BPh_2]$ (**3**),[23] $[(C_5Me_5)_2UH]_2$ (**4**),[24] or $[(C_5Me_5)_2U]_2(\mu$-

η^6:η^6-C_6H_6) (**5**)[23] to yield the stable 20-electron uranium(VI) bis(organoimido) complex $(C_5Me_5)_2U(=N-Ph)_2$ (**6**) (Scheme 1); the analogous group 6 bis(imido) metallocene complexes would be unstable and are not known.

Research by our group has shown that uranium alkyl complexes of the type $(C_5Me_5)_2U(CH_3)(X)$ (X = OTf, Cl), react with diphenyldiazomethane to afford the corresponding 20-electron mono(hydrazonato) complexes $(C_5Me_5)_2U[\eta^2$-(N,N')-$CH_3-N-N=CPh_2](X)$ (eq 1).[25] Additionally, a uranium(IV) hydrazonato complex was obtained from thermolysis of the uranium(VI) bis(imido) complex $(C_5Me_5)_2U(=N-2,4,6$-$^tBu_3$-$C_6H_2)(=N-N=CPh_2)$ and intramolecular C−H addition across the N=U=N core.[26] These results find interesting parallels in group 4 chemistry. For example, Floriani and co-workers[27,28]

$$(1)$$

7

8a, X = OTf
8b, X = Cl
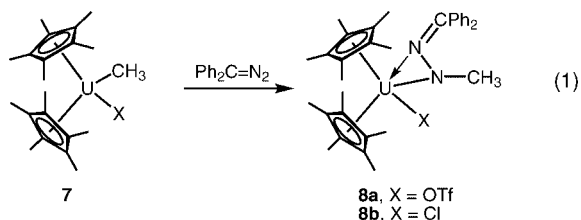
demonstrated that diphenyldiazomethane reacts with $(C_5H_5)_2Zr(H)(Cl)$ by inserting into the Zr−H bond to give the hydrazonato complex $(C_5H_5)_2Zr[\eta^2-(N,N')-H-N-N=CPh_2](Cl)$. Likewise, Santarsiero and Moore[29] reported that $(C_5Me_5)_2Zr(CH_3)(Cl)$ reacts with bis(*p*-tolyl)diazomethane to generate the hydrazonato complex $(C_5Me_5)_2Zr[\eta^2-(N,N')-CH_3-N-N=C(p-tol)_2](Cl)$. A related example was provided by Royo and co-workers,[30] who showed that diphenyldiazomethane inserts into two of the Ti−C bonds of the dimer

$[(C_5Me_5)Ti(CH_3)_2]_2(\mu\text{-O})$ to give the corresponding hydrazonato system $[(C_5Me_5)Ti\{\eta^2-(N,N')-CH_3-N-N=CPh_2\}(CH_3)]_2(\mu\text{-O})$. Recently, the same reaction manifold was used by Evans and co-workers to access lanthanide hydrazonato complexes.[31,32]
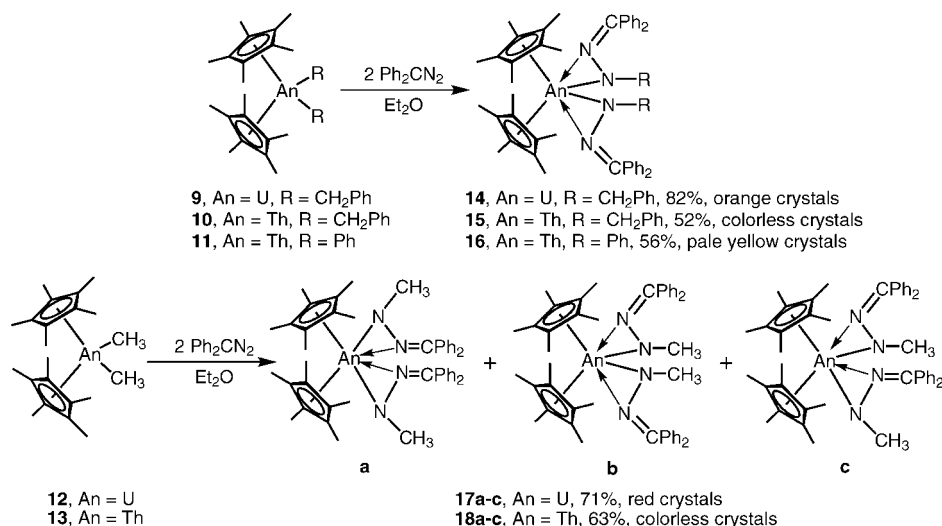
We now report that diazoalkanes readily insert into both metal−carbon bonds of the bis(alkyl) and bis(aryl) complexes $(C_5Me_5)_2AnR_2$ to yield the first bis(hydrazonato) complexes $(C_5Me_5)_2An[\eta^2-(N,N')-R-N-N=CPh_2]_2$ [An = Th, R = CH_3 (**18**), $PhCH_2$ (**15**), Ph (**16**); An = U, R = CH_3 (**17**), $PhCH_2$ (**14**)]. These 20-electron (for Th) and 22-electron (for U) complexes have no transition-metal analogues. In fact, a striking example that highlights this point is provided by the reaction of $(C_5H_5)_2Zr(CH_3)_2$ with excess diphenyldiazomethane, which affords only $(C_5H_5)_2Zr[\eta^2-(N,N')-CH_3-N-N=CPh_2](CH_3)$; the $(C_5H_5)_2Zr$ fragment does not accommodate two η^2-hydrazonato ligands.[27,28] Similarly, reasoning that the larger ionic radius of hafnium could facilitate the access to a d-block metallocene bis(hydrazonato) complex, we examined the reaction of $(C_5Me_5)_2Hf(CH_3)_2$ with excess diphenyldiazomethane; only the mono(hydrazonato) complex $(C_5Me_5)_2Hf[\eta^2-(N,N')-CH_3-N-N=CPh_2](CH_3)$ was observed.[33] Since uranium and thorium complexes possess accessible f valence orbitals whereas zirconium and hafnium complexes do not, these actinide bis(hydrazonato) systems provide a unique platform for investigating f-orbital participation in the reaction chemistry of organometallic compounds. Herein, we describe the synthesis, structures, and electronic properties of these organometallic uranium(IV) and thorium(IV) bis(hydrazonato) complexes. We show that a key factor in directing the chemistry and stabilizing the bis(hydrazonato) actinide structures is the favorable interaction that occurs between the N−N donor molecular orbitals and metal-based 5f and 6d orbitals that are not available in transition metals.

Results and Discussion

1. Synthesis and Structural Characterization. Scheme 2 displays the synthetic methods used and the yields obtained in the preparation of the uranium and thorium bis(hydrazonato)

(1) (a) Tatsumi, K.; Nakamura, A. *J. Organomet. Chem.* **1984**, *272*, 141–154. (b) Pepper, M.; Bursten, B. E. *Chem. Rev.* **1991**, *91*, 719–741. (c) Li, J.; Bursten, B. E. *J. Am. Chem. Soc.* **1997**, *119*, 9021–9032. (d) Diaconescu, P. L.; Arnold, P. L.; Baker, T. A.; Mindiola, D. J.; Cummins, C. C. *J. Am. Chem. Soc.* **2000**, *122*, 6108–6109. (e) Mazzanti, M.; Wietzke, R.; Pecaut, J.; Latour, J.-M.; Maldivi, P.; Remy, M. *Inorg. Chem.* **2002**, *41*, 2389–2399. (f) Meyer, K.; Mindiola, D. J.; Baker, T. A.; Davis, W. M.; Cummins, C. C. *Angew. Chem., Int. Ed.* **2000**, *39*, 3063–3066.

(2) Burns, C. J.; Bursten, B. E. *Comments Inorg. Chem.* **1989**, *9*, 61–93.

(3) While transition-metal complexes tend to obey the 18-electron rule, actinide complexes often have electron counts that exceed 18. For pertinent examples, see: (a) Reynolds, L. T.; Wilkinson, G. *J. Inorg. Nucl. Chem.* **1956**, *2*, 246–253. (b) Fischer, E. O.; Hristidu, Y. *Z. Naturforsch.* **1962**, *173*, 275–276. (c) Streitwieser, A., Jr.; Mueller-Westerhoff, U. *J. Am. Chem. Soc.* **1968**, *90*, 7364. (d) Avdeef, A.; Raymond, K. N.; Hodgson, K. O.; Zalkin, A. *Inorg. Chem.* **1972**, *11*, 1083–1088. (e) Maier, R.; Kanellakopulos, B.; Apostolidis, C.; Meyer, D.; Rebizant, J. *J. Alloys Compd.* **1993**, *190*, 269–271.

(4) For a recent review of the diverse and unusual chemistry concerning reactions promoted by uranium(III) as a reducing agent, see: Evans, W. J.; Kozimor, S. A. *Coord. Chem. Rev.* **2006**, *250*, 911–935.

(5) Arnold, P. L.; Patel, D.; Wilson, C.; Love, J. B. *Nature* **2008**, *451*, 315–318.

(6) Brennan, J. G.; Green, J. C.; Redfern, C. M. *J. Am. Chem. Soc.* **1989**, *111*, 2373–2387.

(7) Burns, C. J.; Eisen, M. S. In *The Chemistry of the Actinide and Transactinide Elements*, 3rd ed.; Morss, L. R., Edelstein, N. M., Fuger, J., Eds.; Springer: Dordrecht, The Netherlands, 2006; Vol. 5, pp 2799–2910.

(8) Diaconescu, P. L.; Cummins, C. C. *J. Am. Chem. Soc.* **2002**, *124*, 7660–7661.

(9) Graves, C. R.; Scott, B. L.; Morris, D. E.; Kiplinger, J. L. *J. Am. Chem. Soc.* **2007**, *129*, 11914–11915.

(10) Graves, C. R.; Yang, P.; Kozimor, S. A.; Vaughn, A. E.; Clark, D. L.; Conradson, S. D.; Schelter, E. J.; Scott, B. L.; Thompson, J. D.; Hay, P. J.; Morris, D. E.; Kiplinger, J. L. *J. Am. Chem. Soc.* **2008**, *130*, 5272–5285.

(11) Hayton, T. W.; Boncella, J. M.; Scott, B. L.; Palmer, P. D.; Batista, E. R.; Hay, P. J. *Science* **2005**, *310*, 1941–1943.

(12) Jantunen, K. C.; Scott, B. L.; Kiplinger, J. L. *J. Alloys Compd.* **2007**, *444−445*, 363–368.

(13) Marks, T. J.; Streitwieser, A. In *The Chemistry of the Actinide Elements*, 2nd ed.; Katz, J. J., Seaborg, G. T., Morss, L. R., Eds.; Chapman and Hall: New York, 1986; Vol. 2, pp 1547−1587.

(14) Maynadie, J.; Berthet, J.-C.; Thuery, P.; Ephritikhine, M. *J. Am. Chem. Soc.* **2006**, *128*, 1082–1083.

(15) Nocton, G.; Pecaut, J.; Mazzanti, M. *Angew. Chem., Int. Ed.* **2008**, *47*, 3040–3042.

(16) Pool, J. A.; Scott, B. L.; Kiplinger, J. L. *Chem. Commun.* **2005**, 2591–2593.

(17) Pool, J. A.; Scott, B. L.; Kiplinger, J. L. *J. Am. Chem. Soc.* **2005**, *127*, 1338–1339.

(18) Schelter, E. J.; Morris, D. E.; Scott, B. L.; Kiplinger, J. L. *Chem. Commun.* **2007**, 1029–1031.

(19) Schelter, E. J.; Yang, P.; Scott, B. L.; Da Re, R. E.; Jantunen, K. C.; Martin, R. L.; Hay, P. J.; Morris, D. E.; Kiplinger, J. L. *J. Am. Chem. Soc.* **2007**, *129*, 5139–5152.

(20) Schelter, E. J.; Yang, P.; Scott, B. L.; Thompson, J. D.; Martin, R. L.; Hay, P. J.; Morris, D. E.; Kiplinger, J. L. *Inorg. Chem.* **2007**, *46*, 7477–7488.

(21) Summerscales, O. T.; Cloke, F. G. *Struct. Bonding (Berlin)* **2008**, *127*, 87–117.

(22) Warner, B. P.; Scott, B. L.; Burns, C. J. *Angew. Chem., Int. Ed.* **1998**, *37*, 959–960.

(23) Evans, W. J.; Kozimor, S. A.; Ziller, J. W. *Chem. Commun.* **2005**, 4681–4683.

(24) Evans, W. J.; Miller, K. A.; Kozimor, S. A.; Ziller, J. W.; DiPasquale, A. G.; Rheingold, A. L. *Organometallics* **2007**, *26*, 3568–3576.

(25) Kiplinger, J. L.; John, K. D.; Morris, D. E.; Scott, B. L.; Burns, C. J. *Organometallics* **2002**, *21*, 4306–4308.

(26) Kiplinger, J. L.; Morris, D. E.; Scott, B. L.; Burns, C. J. *Chem. Commun.* **2002**, 30–31.

(27) Gambarotta, S.; Basso-Bert, M.; Floriani, C.; Guastini, C. *J. Chem. Soc., Chem. Commun.* **1982**, 374–375.

(28) Gambarotta, S.; Floriani, C.; Chiesi-Villa, A.; Guastini, C. *Inorg. Chem.* **1983**, *22*, 2029–2034.

(29) Santarsiero, B. D.; Moore, E. J. *Acta Crystallogr.* **1988**, *C44*, 433–435.

(30) Serrano, R.; Flores, J. C.; Royo, P.; Mena, M.; Pellinghelli, M. A.; Tiripicchio, A. *Organometallics* **1989**, *8*, 1404–1408.

(31) The first lanthanide hydrazonato complex was synthesized by reduction of the azine PhHC=N−N=CHPh by $(C_5Me_5)_2Sm(THF)_2$. See: Evans, W. J.; Drummond, D. K. *J. Am. Chem. Soc.* **1989**, *111*, 3329–3335.

(32) Evans, W. J.; Montalvo, E.; Champagne, T. M.; Ziller, J. W.; DiPasquale, A. G.; Rheingold, A. L. *Organometallics* **2008**, *27*, 3582–3586.

(33) See the Experimental Section and the Supporting Information for further details.

Scheme 1. Synthetic Routes for the Preparation of the Organometallic Uranium(VI) Bis(imido) Complex (C$_5$Me$_5$)$_2$U(=N−Ph)$_2$ (**6**)
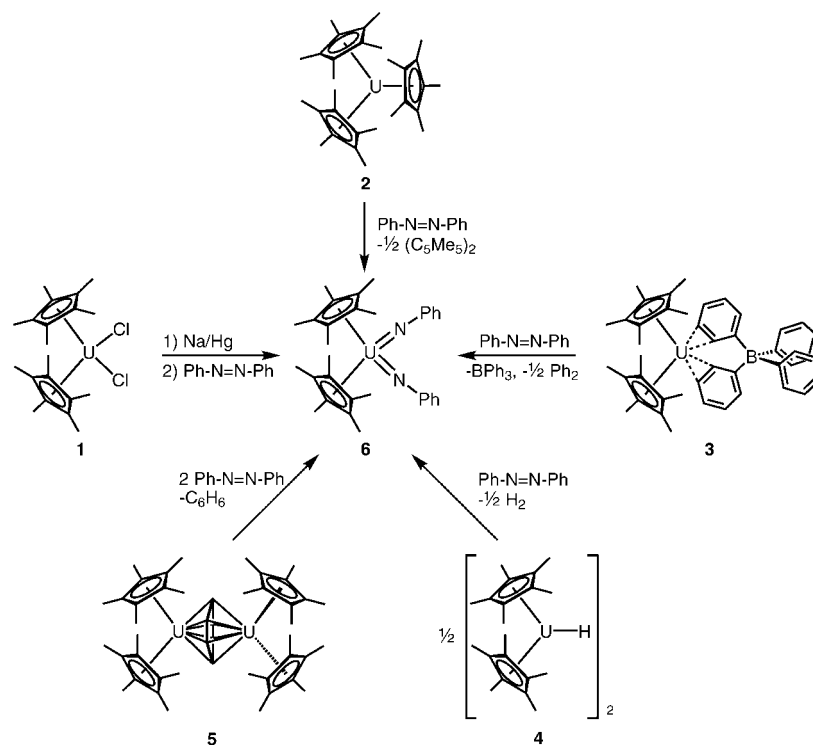
**Scheme 2.** Synthetic Protocol for the Preparation of Uranium and Thorium Bis(hydrazonato) Complexes

9, An = U, R = CH$_2$Ph
10, An = Th, R = CH$_2$Ph
11, An = Th, R = Ph

14, An = U, R = CH$_2$Ph, 82%, orange crystals
15, An = Th, R = CH$_2$Ph, 52%, colorless crystals
16, An = Th, R = Ph, 56%, pale yellow crystals

12, An = U
13, An = Th

17a-c, An = U, 71%, red crystals
18a-c, An = Th, 63%, colorless crystals

complexes. Treatment of a diethyl ether solution of the bis(alkyl) or bis(aryl) actinide complexes **9**–**13** with excess diphenyldiazomethane (2.5 equiv) gives the corresponding uranium(IV) and thorium(IV) bis(hydrazonato) complexes **14**–**18** as crystalline solids in 52–82% isolated yields. The modest isolated yields reflect the high solubility of the bis(hydrazonato) complexes rather than the formation of any byproducts. Indeed, when the reactions were monitored by ^{1}H NMR spectroscopy, compounds **14**–**18** were the only observable actinide-containing products and were formed in greater than 95% yield. These migratory insertion reactions proceed rapidly at room temperature. Addition of 1 equiv of diphenyldiazomethane does not generate the mono(hydrazonato) alkyl complex but rather generates a mixture of the bis(alkyl) and bis(hydrazonato) complexes, suggesting that the second diazoalkane insertion is faster than the first insertion. Following workup, all of the complexes were repro-

ducibly isolated as analytically pure solids and characterized by a combination of NMR, UV−visible, and near-IR spectroscopy, electrochemistry, elemental and mass spectrometric analyses, and X-ray crystallography.

These actinide bis(hydrazonato) complexes display NMR spectra typical of uranium(IV) and thorium(IV) organometallic complexes. In particular, the ^{1}H NMR spectra of the 6d^{0}5f^2 U^{IV} complexes **14** and **17** are sharp and paramagnetically shifted,[34] whereas the thorium compounds **15**, **16**, and **18** display sharp NMR resonances consistent with a diamagnetic 6d^{0}5f^0 Th^{IV} metal center. For the uranium and thorium benzyl- and phenyl-substituted bis(hydrazonato) complexes **14**–**16**, only one species is observed in solution, but ^{1}H NMR spectroscopy suggests that

(34) Marks, T. J.; Seyam, A. M.; Kolb, J. R. *J. Am. Chem. Soc.* **1973**, *95*, 5529–5539.
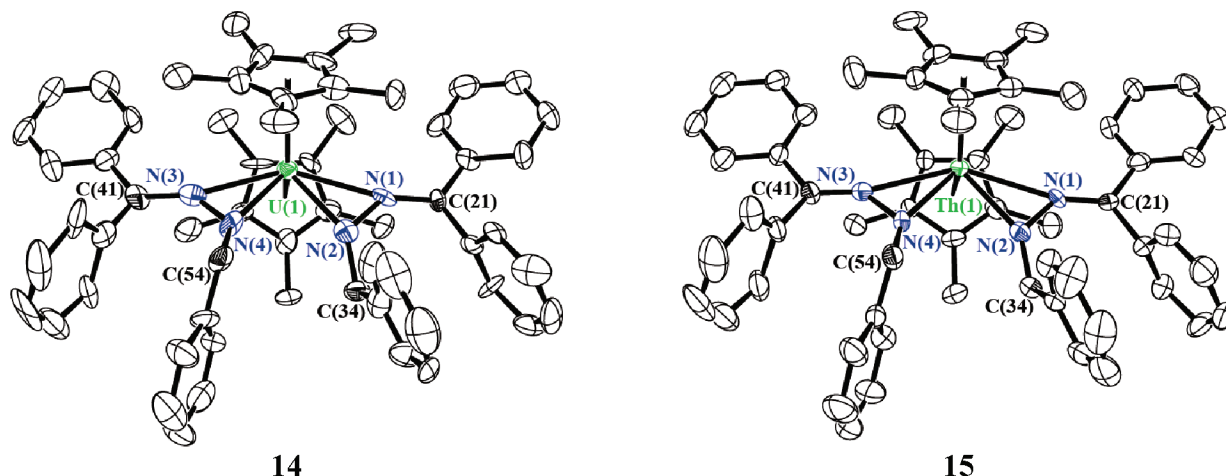
Figure 1. Molecular structures of complexes **14** (left) and **15** (right), with thermal ellipsoids at the 50% level. Hydrogen atoms have been omitted for clarity.
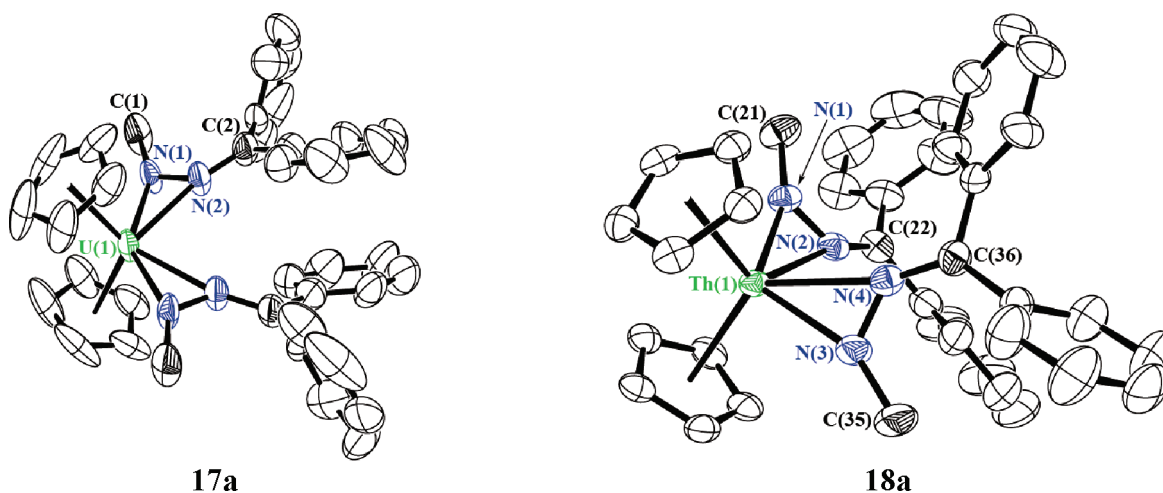
Figure 2. Molecular structures of complexes **17a** (left) and **18a** (right), with thermal ellipsoids at the 50% probability level. Hydrogen atoms and the methyl groups of the C_5Me_5 ligands have been omitted for clarity.

the methyl-substituted bis(hydrazonato) complexes **17** and **18** exist as an equilibrium mixture of isomers. For example, complex **17** shows three distinct C_5Me_5-containing species that are present in a 2:5:3 ratio at ambient temperature, and partial coalescence is observed when a solution of the complexes is heated to 110 °C. Isolation of **17a** as single crystals (see below) followed by solvation in C_6D_6 and analysis by ^1H NMR spectroscopy showed a similar 2:5:3 ratio of products, suggesting that **17a–c** interconvert by rotation about the U−NCH₃ bonds to arrive at the thermodynamic equilibrium. Similar results were obtained for the thorium complex **18**.

X-ray diffraction studies confirmed the identity of the U^{IV} and Th^{IV} bis(hydrazonato) complexes (Figures 1 and 2). Table 1 presents salient geometric parameters for complexes **14**, **15**, **17a**, and **18a**. The molecular structures of all four 10-coordinate complexes feature two η^2-(N,N′)-bound hydrazonato moieties, $Ph_2C=N−N−R$ (R = CH_3, CH_2Ph), which are positioned in the equatorial girdle of the $(C_5Me_5)_2An$ (An = Th, U) bent-metallocene framework. Each η^2-(N,N′)-hydrazonato ligand interacts with the actinide metal center to form an An−N σ bond and an An−N dative interaction, which result from the 1,2-insertion of diphenyldiazomethane into both An−C bonds. Similar coordination modes have been observed in related 10-coordinate bis(pentamethylcyclopentadienyl) uranium(IV) com-

plexes featuring η^2-acyl,[35] η^2-carbamoyl,[36] η^2-acetate,[37] and η^2-pyrazolate[38] ligands.

For the methyl-substituted bis(hydrazonato) complexes (**17a** and **18a**), the η^2-hydrazonato ligands are rotated out of the equatorial girdle to a greater extent than for the benzyl-substituted bis(hydrazonato) complexes (**14** and **15**). For example, in the thorium complex **18a**, the η^2-hydrazonato ligands are twisted relative to the equatorial plane of the bent metallocene by $\theta_1 = 42.2°$ and $\theta_2 = 40.5°$ ($\theta_{ave} = 41.4°$). The η^2-hydrazonato ligands in the uranium analogue **17a** are also rotated, albeit to a lesser extent ($\theta_{ave} = 13.2°$). In contrast to the methyl derivatives, the benzyl-substituted bis(hydrazonato) complexes possess shorter An−N$_{amide}$ bonds between the metal and the "internal" nitrogens, where the crowding is the greatest, while the longer An−N$_{dative}$ bonds are those from the metal to the "external" nitrogens, where the crowding is minimized. In the uranium complex **14**, the η^2-hydrazonato ligands are twisted by only $\theta_{ave} = 6.1°$. Similarly, for the thorium complex **15**, the

(35) Moloy, K. G.; Marks, T. J. *J. Am. Chem. Soc.* **1984**, *106*, 7051–7064.
(36) Fagan, P. J.; Manriquez, J. M.; Vollmer, S. H.; Day, C. S.; Day, V. W.; Marks, T. J. *J. Am. Chem. Soc.* **1981**, *103*, 2206–2220.
(37) Moloy, K. G.; Marks, T. J. *Inorg. Chim. Acta* **1985**, *110*, 127–131.
(38) Eigenbrot, C. W.; Raymond, K. N. *Inorg. Chem.* **1982**, *21*, 2653–2660.

Table 1. Geometric Parameters for Complexes **14**, **15**, **17a**, and **18a** from X-ray Diffraction Data

	14 (M = U, R′ = Ph)	**15** (M = Th, R′ = Ph)	**17a** (M = U, R′ = H)	**18a** (M = Th, R′ = H)
		Distances (Å)		
M−N	2.526(16)	2.571(7)	2.317(8)	2.338(4)
	2.285(16)	2.339(7)	2.469(8)	2.552(4)
	2.506(17)	2.578(8)		2.352(4)
	2.275(17)	2.323(8)		2.554(4)
N−N	1.37(2)	1.350(10)	1.308(11)	1.344(6)
	1.35(2)	1.359(10)		1.345(6)
N−C(CPh$_2$)	1.36(2)	1.283(11)	1.310(14)	1.289(6)
	1.32(2)	1.286(11)		1.292(6)
N−C(CH$_2$R′)	1.51(2)	1.420(12)	1.464(13)	1.464(7)
	1.49(2)	1.455(11)		1.452(7)
Ct−M^a	2.699	2.682	2.526	2.591
	2.585	2.595		2.593
		Angles (deg)		
M−N−N	83.5(10)	83.8(5)	83.5(10)	65.4(3)
	83.3(11)	84.6(5)		66.0(2)
N−N−C(CPh$_2$)	130.3(17)	130.4(8)	130.7(9)	131.0(5)
	130.6(16)	130.3(7)		130.2(4)
N−N−C(CH$_2$R′)	123.7(16)	123.7(7)	123.0(9)	122.1(4)
	123.4(15)	124.2(7)		122.1(4)
M−N−C(CPh$_2$)	165.4(12)	165.0(6)	161.0(8)	163.6(4)
	165.2(14)	165.7(6)		163.9(3)
M−N−C(CH$_2$R′)	146.6(12)	148.5(6)	154.0(8)	154.5(4)
	148.6(13)	148.4(6)		154.6(4)
Ct−M−Ct^a	134.4	134.8	128.5	122.9

^{a} Ct = C$_5$Me$_5$ centroid.

N(1)−Th(1)−N(2) and N(3)−Th(1)−N(4) planes are twisted by only θ_{ave} = 6.5°.

$\theta_{ave} = 1/2(\theta_1 + \theta_2)$
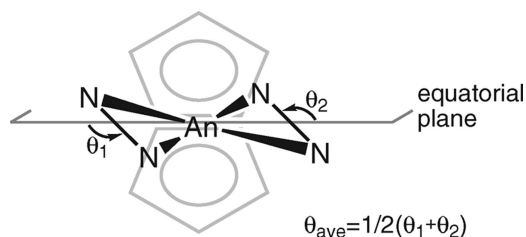
The U−N$_{amide}$ bond distances in **14** [U(1)−N(2) = 2.285(16) Å, U(1)−N(4) = 2.275(17) Å] lie at the high end of the range for other structurally characterized uranium(IV) amide complexes,[39] which most likely results from of the steric congestion around the 10-coordinate uranium(IV) metal center. At 1.32(2) and 1.36(2) Å, respectively, the N(1)−C(21) and N(3)−C(41) bond lengths are somewhat longer than the theoretical N≡C double-bond distance of 1.279 Å.[40] Furthermore, the N(1)−N(2) bond length of 1.37(2) Å and the N(3)−N(4) bond length of 1.35(2) Å are intermediate between the lengths of N−N single and N≡N double bonds (1.425 and 1.240 Å, respectively),[40] implying electronic delocalization over the C−N−N units. The C−N−N binding parameters reported herein compare well with the metrical parameters reported for the Ph$_2$C≡N−N−CH$_3$ moieties in the mono(hydrazonato) uranium(IV) complexes (C$_5$Me$_5$)$_2$U[η^2-(*N,N′*)-CH$_3$−N−N≡CPh$_2$](X) [X = OTf (**8a**):

C−N = 1.32(3) Å, N−N = 1.41(3) Å; X = Cl (**8b**): C−N = 1.310(11) Å, N−N =1.370(9) Å],[25] the Ph$_2$C≡N−N−CH$_2$ fragment in (C$_5$Me$_5$)$_2$U{η^3-(*N,N′,N″*)-[N(H)(2,4-^{t}Bu$_2$-C$_6$H$_2$-6-CH$_2$−N−N≡CPh$_2$)]} [C−N = 1.325(16) Å, N−N = 1.364(13) Å],[26] and the (Me$_3$Si)(H)C≡N−N−CH$_2$ units in the related lanthanide mono(hydrazonato) complexes (C$_5$Me$_5$)$_2$Ln[η^2-(*N,N′*)-C$_3$H$_5$−N−N≡C(H)(SiMe$_3$)] [Ln = Sm: C−N = 1.338(12) Å, N−N = 1.333(10) Å; Ln = La: C−N = 1.310(3) Å, N−N = 1.343(3) Å].[32] The thorium(IV) benzyl-substituted bis(hydrazonato) complex **15** is essentially isostructural to complex **14**, with the differences in analogous An−ligand bond lengths being readily attributed to the 0.05 Å smaller ionic radius of U^{IV} compared with Th^{IV}.[41] The Th−N$_{amide}$ bond distances found in **15** [Th(1)−N(2) = 2.339(7) Å, Th(1)−N(4) = 2.323(8) Å] also agree well with those found for other thorium(IV) amide complexes.[42] Complexes **17a** and **18a** were subjected to scrutiny by X-ray crystallography (Figure 2) and found to possess metrical parameters comparable to those of the benzyl complexes **14** and **15**, respectively.

2. Theoretical Study. Density functional theory (DFT) calculations were performed to gain insight into the electronic structure of the thorium and uranium bis(hydrazonato) complexes. Furthermore, the migratory insertion of Ph$_2$CN$_2$ into *both* metal−carbon bonds of the bis(alkyl) or bis(aryl) complexes (C$_5$Me$_5$)$_2$MR$_2$ is unique to the actinides (M = Th, U) and is not

(39) For representative examples of uranium(IV) complexes containing a U−N$_{amide}$ linkage, see: (a) Cp$_3$U[N(C$_6$H$_5$)$_2$], U−N = 2.29(1) Å: Cramer, R. E.; Engelhardt, U.; Higa, K. T.; Gilje, J. W. *Organometallics* **1987**, *6*, 41–45. (b) (C$_5$Me$_5$)$_2$U[NH(2,6-Me$_2$-C$_6$H$_3$)]$_2$, U−N = 2.267(6) Å: Straub, T.; Frank, W.; Reiss, G. J.; Eisen, M. S *J. Chem. Soc., Dalton Trans.* **1996**, 2541–2546. (c) [Me$_2$Si(η^5-C$_5$Me$_4$)(^{t}BuN)]U(NMe$_2$)$_2$, U−N = 2.278(4), 2.207(4), 2.212(4) Å: Stubbert, B. D.; Stern, C. L.; Marks, T. J. *Organometallics* **2003**, *22*, 4836–4838.

(40) Allen, F. H.; Kennard, O.; Watson, D. G.; Brammer, L.; Orpen, A. G.; Taylor, R. *J. Chem. Soc., Perkin Trans. 2* **1987**, S1–S19.

(41) Shannon, R. D. *Acta Crystallogr.* **1976**, *A32*, 751–767.

(42) For representative examples of thorium(IV) complexes containing a Th−N$_{amide}$ linkage, see: (a) (η^3-BH$_4$)Th[N(SiMe$_3$)$_2$]$_3$, Th−N$_{ave}$ = 2.32(2) Å: Turner, H. W.; Andersen, R. A.; Zalkin, A.; Templeton, D. H. *Inorg. Chem.* **1979**, *18*, 1221–1224. (b) (C$_5$Me$_5$)$_2$Th(Cl)(C$_6$N$_3$), Th−N$_{ave}$ = 2.46(1) Å: Sternal, R. S.; Sabat, M.; Marks, T. J. *J. Am. Chem. Soc.* **1987**, *109*, 7920–7921. (c) (η^8-C$_8$H$_8$)Th[N(SiMe$_3$)$_2$]$_2$, Th−N$_{ave}$ = 2.34(1) Å: Gilbert, T. M.; Ryan, R. R.; Sattelberger, A. P. *Organometallics* **1988**, *7*, 2514–2518. (d) [N(SiMe$_3$)$_2$]$_2$Th(NMePh)$_2$, Th−N$_{ave}$ = 2.308(7) Å: Barnhart, D. M.; Clark, D. L.; Grumbine, S. K.; Watkin, J. G. *Inorg. Chem.* **1995**, *34*, 1695–1699. (e) [(CGC)Th[N(SiMe$_3$)$_2$](μ-Cl)]$_2$, Th−N = 2.335(5) and 2.334(5) Å: Stubbert, B. D.; Marks, T. J. *J. Am. Chem. Soc.* **2007**, *129*, 6149–6167.

Scheme 3. Reaction Scheme for the Theoretical Analysis of the Formation of the Bis(hydrazonato) Complexes $(C_5H_5)_2M[\eta^2\text{-}(N,N')\text{-}CH_3-N-N=CH_2]_2$ (**M-II**, M = Th, U, Zr) from the Reaction between $(C_5H_5)_2M(CH_3)_2$ and H_2CN_2
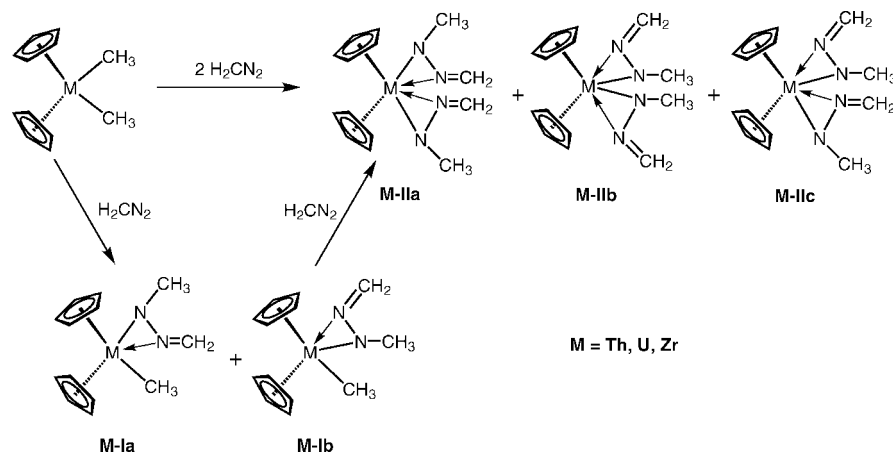
observed for the structurally related transition-metal systems (M = Zr, Hf). The reasons for the differences between the reactivities of d- and f-block metallocenes were also investigated, with special attention devoted to the influence of 5f orbitals on the thermodynamics and kinetics of this reaction manifold.

2.1. Structural Results. As the electronic absorption spectroscopy and voltammetry studies conducted on the uranium and thorium bis(hydrazonato) complexes **14−18** show (see below), the substituents on the hydrazonato ligand have only a minor impact on the electronic structure of the complexes. In view of this, calculations were performed on the model complexes $(C_5H_5)_2M[\eta^2\text{-}(N,N')\text{-}CH_3-N-N=CH_2]_2$ (**M-II**, M = Th, U, Zr), in which the C_5Me_5 ligands were replaced by C_5H_5 for further comparison with previous studies.[43] The reaction sequence for the theoretical analysis is shown in Scheme 3, and the calculated structures, geometric parameters, and energies for the bis(hydrazonato) complexes **Th-IIa−c** and **U-IIa−c** are given in Figure 3. Greater convergence difficulties in the DFT calculations can occur for actinide complexes with unpaired electrons than for closed-shell actinide species. These arise primarily from the determination of which combination of two "α spin" orbitals are occupied (in the case of U complexes with a $5f^2$ configuration) within the relatively closely spaced 5f manifold.

Overall, the optimized geometries are in good agreement with the available X-ray diffraction results. For example, the average calculated (2.29 Å, **U-IIb**) and experimental (2.29 Å, **14**) bond lengths for the U−N_{amide} bonds are within 0.01 Å of each other. Although the calculated bond distance for the longer U−N_{dative} interaction (2.49 Å, **U-IIb**) is underestimated by 0.03 Å, the N−N bond distance (1.37 Å, **U-IIb**) compares well with that observed for **14** (1.36 Å ave). Similarly, as Figure 3 shows, the calculated geometries for **U-IIa**, **Th-IIa**, and **Th-IIb** compare well with the structures obtained for their experimental counterparts (**17a**, **18a**, and **15**, respectively).

Also of interest is the orientation of the four nitrogen atoms of the two hydrazonato ligands. Whereas in isomer **M-IIb** the two hydrazonato ligands are almost coplanar (the angle θ_{ave} between the two N_1−M−N_2 planes is close to zero), the isomers **M-IIa** and **M-IIc** feature highly twisted ligands, with the N atoms significantly displaced out of the equatorial plane of the metallocene. The same twist is observed experimentally. For

example, complexes **14** and **15** display a nearly coplanar orientation of the hydrazonato ligands (θ_{ave} = 6.1 and 6.5° compared with the calculated 0.3 and 2.3° for **U-IIb** and **Th-IIb**, respectively). The measured twist angles in **17a** and **18a** are θ_{ave} = 13.2 and 41.4°, respectively, compared to the calculated values of 75.6° (**U-IIa**) and 74.1° (**Th-IIa**). It is important to point out that the thermodynamic stabilities of the six isomers considered (**Th-IIa−c** and **U-IIa−c**) are not influenced by the twist angles, as the energies of the optimum structures are within ±0.6 kcal/mol of one another for the thorium system and ±2.9 kcal/mol for uranium. This is fully consistent with the ^1H NMR experiments for the methyl-substituted bis(hydrazonato) complexes **17a−c** and **18a−c**, where a mixture of species was observed at room temperature (see above).

2.2. Electronic Structure. The electronic structure of the actinide bis(hydrazonato) complexes arises from the interaction of a $[(C_5H_5)_2An]^{2+}$ fragment with two negatively (−1) charged $\eta^2\text{-}(N,N')$-hydrazonato ligands. The bonding interactions in $(C_5H_5)_2M$ metallocene systems are very well-known for the transition metals, in which there are three frontier molecular orbitals (MOs) on the metal that are centered in the equatorial plane (σ_1, σ_2, and σ_3, shown on the left-hand side in Figure 4) available for bonding.[44−46] For group 4 metals, this leads to coordinatively and electronically saturated 18-electron d^0 $(C_5H_5)_2ML_3$ complexes. As illustrated in Figure 4, the coordination of a fourth ligand in the wedge of the metallocene requires the stabilization of an antisymmetric combination of the ligand orbitals (σ_4). Because of symmetry constraints, an f orbital is better suited to accommodate this fourth ligand. For bent metallocenes, such a situation can only be achieved with actinides, where both 6d and 5f atomic orbitals (AOs) are available for bonding interactions.[47] A second difference is the larger ionic radii of actinides compared with transition metals,

(44) Bursten, B. E.; Strittmatter, R. J. *Angew. Chem., Int. Ed. Engl.* **1991**, *30*, 1069–1085.

(45) Green, J. C. *Chem. Soc. Rev.* **1998**, *27*, 263–271.

(46) Lauher, J. W.; Hoffmann, R. *J. Am. Chem. Soc.* **1976**, *98*, 1729–1742.

(47) A historical account of approaches to the bonding in $(C_5H_5)_2An$ complexes and related species has been given by Bursten and Strittmatter.[44] The additional possibilities provided by f-orbital interactions in bent-metallocene uranium(IV) bis(pyrazolate) and bis(acyl) complexes were noted by Tatsumi and Nakamura; see:(a) Tatsumi, K.; Nakamura, A.; Hofmann, P.; Hoffmann, R.; Moloy, K. G.; Marks, T. J. *J. Am. Chem. Soc.* **1986**, *108*, 4467–4476. (b) Tatsumi, K.; Nakamura, A. *Inorg. Chim. Acta* **1987**, *139*, 247–251.

(43) Hay, P. J. *Organometallics* **2007**, *26*, 4424–4431.
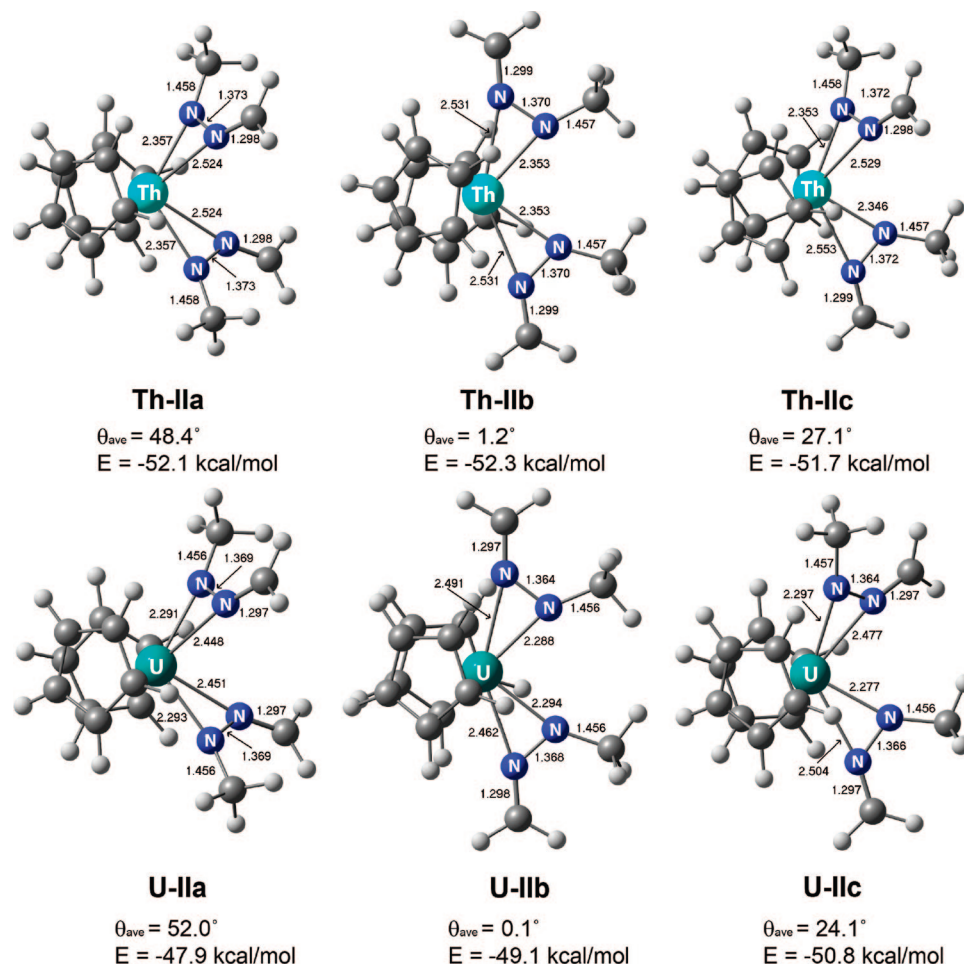
Figure 3. Optimized geometries of the actinide bis(hydrazonato) complexes **Th-IIa**−**c** and **U-IIa**−**c**. The energy reference points are [**Th-Ia** + H_2CN_2] and [**U-Ia** + H_2CN_2], respectively.
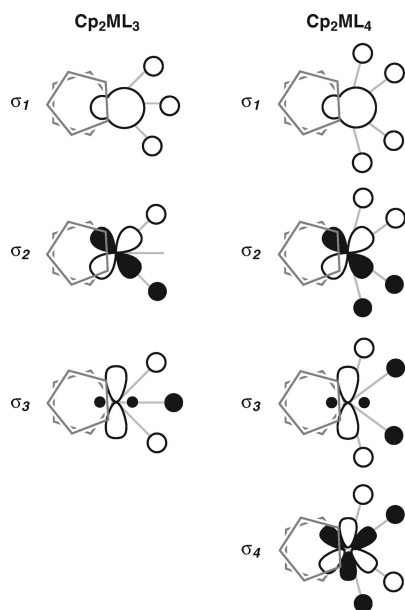
Figure 4. Pictorial representations of the highest occupied MOs describing the M−L σ-bonding interactions in $(C_5H_5)_2ML_3$ and $(C_5H_5)_2ML_4$ complexes.

which also allows for a higher coordination number (up to 12) compared with their transition-metal counterparts.

The bonding in the bis(hydrazonato) complexes **Th-IIb** and **U-IIb** was examined by analyzing the actinide−ligand interactions in the valence orbitals of the complexes and compared with the bonding in the structurally related transition-metal system **Zr-IIb** (Figures 5 and 6).[48]

In the three **M-IIb** complexes, the highest occupied MOs consist of σ_{M-N}, π_{M-Cp}, and π_{M-N} bonding interactions (Figure 5). The electronic structures of **U-IIb** and **Th-IIb** are very similar, the main difference arising from the presence of two singly occupied metal-centered MOs (>80% electronic density on U) of 5f character (99%) for **U-IIb**, consistent with a $5f^2$ U^{IV} metal center. The σ_1, σ_2, σ_3, and σ_4 orbitals describe the σ-bonding character in the four M−N bonds. Participation from the metal center in these four orbitals ranges from ∼8 to ∼13% for both **Th-IIb** and **U-IIb**. From Figure 5, the contribution of the metal to σ_1, σ_2, and σ_3 mainly features 6d character, which ranges from 63.0 to 91.6% for **Th-IIb** and 55.0 to 76.7% for **U-IIb**.

At this point, σ_4 deserves some special attention. This MO is composed of the totally antisymmetric combination of the nitrogen lone pairs (90.8% for **Th-IIb**; 89.5% for **U-IIb**) and a

(48) Complexes **M-IIb** possess a planar orientation of the two η^2-hydrazonato ligands ($\theta_{ave} \approx 0°$) that allows for a better σ/π separation, thereby facilitating the description of the bonding scheme. However, we also show that the twist between the hydrazonato ligands observed in isomers **M-IIa** and **M-IIc** (M = Th, U, Zr) does not affect the overall metal−ligand interactions in these complexes.
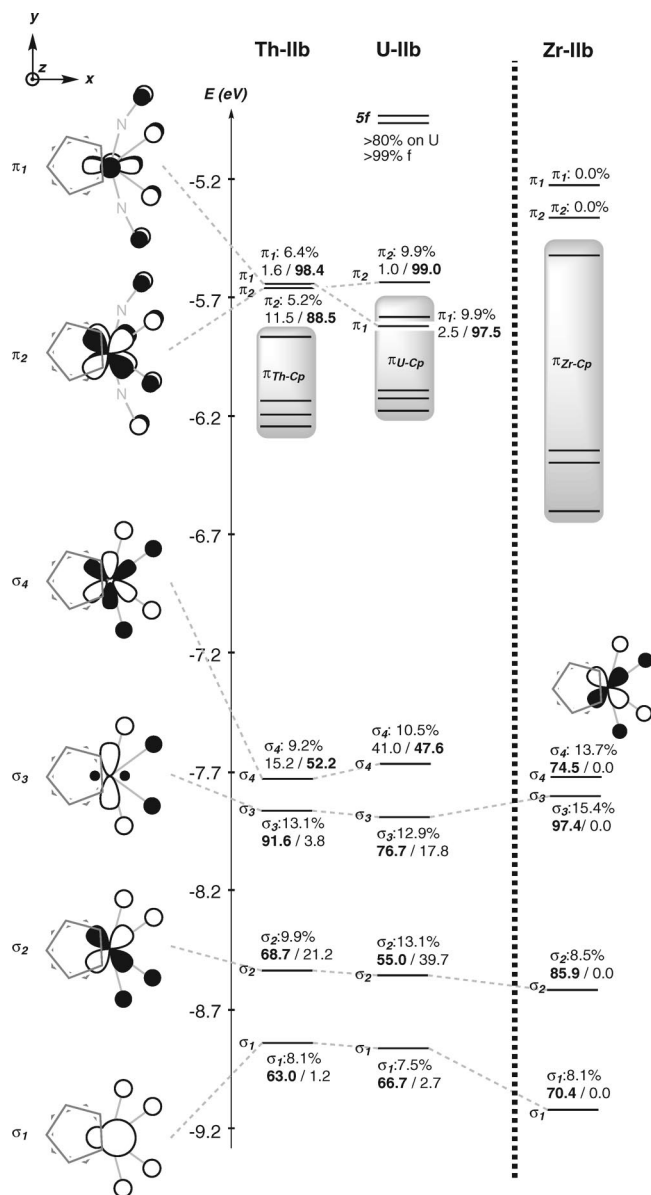
Figure 5. Diagram illustrating the highest occupied MOs for complexes **M-IIb** (M = Th, U, Zr). For each MO, the first number represents the participation (%) of the metal AOs in the considered MO, and the two consecutive numbers that follow report the contribution (%) of the 6d and 5f AOs to the metal hybrid orbital (e.g., π_1 in **Th-IIb** consists of 93.6% ligand-based and 6.4% metal-based components, for which the breakdown of the metal contributions is 1.6% 6d and 98.4% 5f character.)

metal hybrid orbital (9.2% for **Th-IIb**; 10.5% for **U-IIb**). Figure 5 shows that this interaction is favored with increasing 5f admixture to the metal hybrid orbital. In **Th-IIb**, the metal hybrid orbital indeed consists of 52.2% 5f character oriented toward the four nitrogen atoms (in σ_4), with the 6d character limited to 15.2%. The same interaction occurs in **U-IIb**, where the metal contribution to σ_4 has 47.6% 5f character.

The M−N π system in **Th-IIb** and **U-IIb** is made of two MOs, π_1 and π_2, having somewhat higher metal participation for uranium (9.9% in **U-IIb**) than for thorium (5.2−6.4% in **Th-IIb**). In both complexes, the metal orbital is almost a pure 5f orbital (88.5−99.0%). Specifically, $5f_{xy^2}$ is involved in π_1 and $5f_{xyz}$ in π_2, clearly demonstrating a noticeable involvement of 5f orbitals in the stabilization of the actinide bis(hydrazonato) complexes.

No f orbitals are available for bonding interactions in **Zr-IIb**. The three lowest-energy σ MOs in this system (σ_1, σ_2, σ_3) present features similar to those found in **Th-IIb** and **U-IIb**, with comparable contributions from the metal AOs (8.1−15.4%) that have fairly large d character (70.4−97.4%). The main difference between **Th-IIb**/**U-IIb** and **Zr-IIb** appears in σ_4. In the actinide complexes, this MO is better stabilized by the admixture of 5f orbitals [$5f_{x(x^2−3y^2)}$] on the metal center. In **Zr-IIb**, on the other hand, stabilization of σ_4 (13.7% metal, 74.5% 4d character) is provided by a 4d orbital with the correct symmetry (d_{xy}; the same AO is used for the stabilization of σ_2). As mentioned above, the actinide 5f orbitals in **U-IIb** and **Th-IIb** are also critical for stabilizing the hydrazonato ligand π orbitals. This is fully confirmed by an examination of the $\pi_{Zr−N}$ system in **Zr-IIb**. As depicted for this case in Figure 5, both π_1 and π_2 are totally ligand-centered and possess no metal character, which confirms that Zr cannot compensate for the absence of 5f orbitals by using 4d orbitals to stabilize the ligand π orbitals. While d orbitals such as d_{xz} could be invoked to stabilize π_1 and π_2, they lie much higher in energy in the $(C_5H_5)_2Zr$ fragment and are strongly involved in the $\pi_{Zr−Cp}$ interactions.

To summarize, the MO diagrams of the bis(hydrazonato) complexes **Th-IIb** and **U-IIb** exhibit similar features. In particular, in both complexes the 5f orbitals are clearly involved in accommodating the fourth ligand in the equatorial wedge of the metallocene and stabilizing the occupied π orbitals on the η^2-hydrazonato ligands. In the zirconium complex **Zr-IIb**, σ_4 is partially stabilized by a 4d orbital, but π_1 and π_2 remain pure ligand orbitals and possess no metal character.

The overall electronic distributions for **Th-IIa−c**, **U-IIa−c**, and **Zr-IIb** obtained from Mulliken analysis are given in Table 2. For a given metal, the electronic distribution is not affected by the isomer considered (**a**, **b**, or **c**), and the twisting of the two η^2-hydrazonato ligands observed in **M-IIa** and **M-IIc** mixes the σ and π interactions without any impact on the overall electronic distribution of the system. For example, the contribution of the 5f orbitals in **Th-IIa** and **Th-IIc** is distributed over the full MO diagram instead of being concentrated in only three MOs (σ_4, π_1, and π_2) as in **Th-IIb**. This is in accord with the small energy differences separating these isomers, as is observed experimentally. Furthermore, the uranium complexes **U-IIa−c** have a 5f population that is ~2 electrons larger than that in the thorium complexes **Th-IIa−c**, which is consistent with the additional unpaired 5f electrons in the U^{IV} complexes. The ligand-to-metal charge transfer (LMCT) leading to increased 5f occupancies (compared with the formal An^{4+} ion) therefore has a similar magnitude for the thorium and uranium complexes. Overall, the population analysis gives net charges of about +1.34 and +1.37 for the bis(hydrazonato) complexes **Th-IIa−c** and **U-IIa−c**, respectively. Thus, these complexes are more ionic than the corresponding $(C_5H_5)_2An(CH_3)_2$ complexes, where the computed charge on the metal is +0.77 (An = Th) and +1.07 (An = U), which is consistent with the greater electronegativity of the N-containing η^2-hydrazonato ligands compared with methyl ligands.[49]

While the Mulliken analysis gives a picture of the electronic structure that is in between purely ionic and covalent, natural bond orbital (NBO) analysis gives a more ionic view.[50] For the

(49) Yang, P.; Warnke, I.; Martin, R. L.; Hay, P. J. *Organometallics* **2008**, *27*, 1384–1392.

(50) Glendening, E. D.; Badenhoop, F. K.; Reed, A. E.; Carpenter, J. E.; Bohmann, J. A.; Morales, C. M.; Weinhold, F. *NBO 5.0*; Theoretical Chemistry Institute, Univeristy of Wisconsin: Madison, WI, 2001.
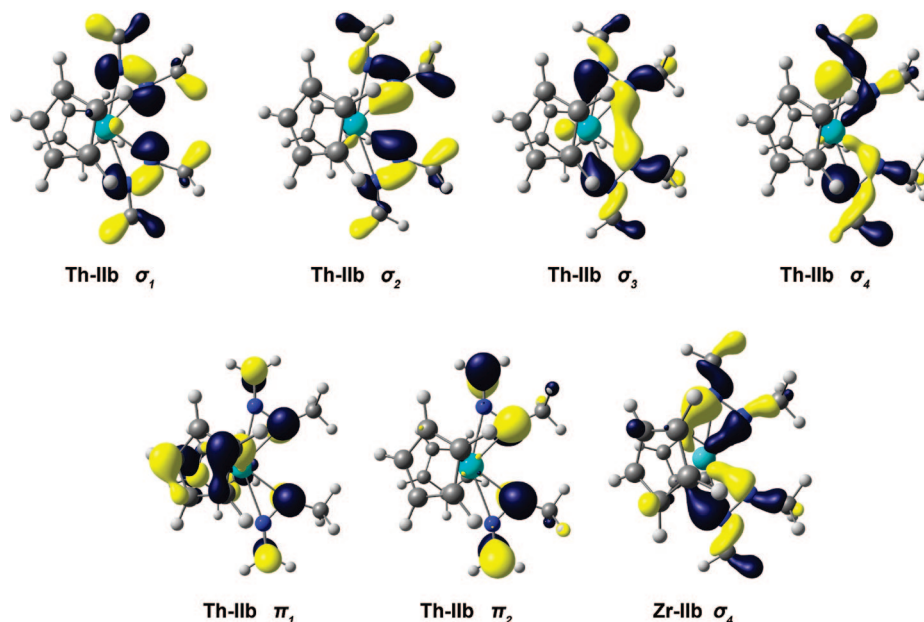
Figure 6. Relevant occupied MOs for the bis(hydrazonato) complexes **Th-IIb** and **Zr-IIb**.

Table 2. Calculated Mulliken Populations for the Bis(hydrazonato) Complexes **U-IIa**−**c**, **Th-IIa**−**c**, and **Zr-IIb**

complex	charge	7s, 7p	6d	5f	5s, 5p	4d
Th-IIa	+1.34	0.38	1.52	0.76		
Th-IIb	+1.35	0.39	1.50	0.76		
Th-IIc	+1.34	0.37	1.51	0.78		
U-IIa	+1.37	0.17	1.71	2.75		
U-IIb	+1.35	0.19	1.70	2.76		
U-IIc	+1.37	0.25	1.66	2.72		
Zr-IIb	+1.33				0.72	1.95

model complexes **U-IIb** and **Th-IIb**, the NBO analysis gives U a charge of +1.59 with a configuration of $(7s,7p)^{0.14}(6d)^{1.30}(5f)^{2.96}$ and Th a charge of +1.69 with a configuration of $(7s,7p)^{0.44}(6d)^{1.31}(5f)^{0.56}$. This population analysis allows for a localized description of each M−N bond. In **Th-IIb**, the metal contribution reaches 7.0% for the Th−NCH$_3$ amide σ bonds (with 26.2% 5f character) and 5.8% for the dative Th−NCH$_2$ σ bonds (with 31.5% 5f character). The polarization of the M−N bonds is even less marked for the uranium complex **U-IIb**, in which the metal-center participation is 12.2% in the U−NCH$_3$ amide σ bonds (with 24.4% 5f character) and 9.9% in the dative U−NCH$_2$ σ bonds (with 45.5% 5f character). These results are in complete agreement with the gross population analysis of the MO diagrams presented in Figure 5.[51]

The virtual (vacant) orbitals for the uranium and thorium bis(hydrazonato) complexes were examined to guide in the interpretation of the spectroscopic results for complexes **14** and **15** (see below). The full experimental structures **14** and **15** were used in these calculations to include the effect that electronic delocalization over the phenyl rings has on the transition energies as well as the possibility of ligand-localized $\pi_{(Ph)} \rightarrow \pi^*_{(Ph)}$ transitions. While more quantitative predictions of excited-state energies for complexes possessing closed-shell ground states are possible using time-dependent DFT calculations,[52] in

the present work the orbital-energy differences were examined in a more qualitative manner to compare the electronic excitations in the closed-shell Th^{IV} and open-shell U^{IV} complexes. On the whole, the MO diagrams for both **15** and **14** derive directly from those of their model complexes **Th-IIb** and **U-IIb**, respectively,[53] and can be described by blocks of orbitals. The highest occupied levels of **15** correspond to $\sigma_{(Th-N)} < \pi_{(Ph)} < \pi_{(Th-N)} < \pi_{(Th-C_5Me_5)}$. In addition to the corresponding set of levels for complex **14**, there are two partially occupied 5f levels lying at higher energies. The virtual levels of **15** appear in the order $\pi^*_{(Th-N)} < \pi^*_{(Ph)} < 5f_{(Th)}$, while for **14** the levels appear as $5f_{(U)}$ (partially occupied) $< \pi^*_{(U-N)} < \pi^*_{(Ph)}$. For the thorium complex **15**, the lowest-energy transition would involve the excitation of one electron from the $\pi_{(Th-C_5Me_5)}$ block to the vacant $\pi^*_{(Th-N)}$ MOs. According to the energy gap between these two sets of MOs, this transition roughly requires an energy of 31 000 cm^{-1}. The second transition also exhibits $\pi \rightarrow \pi^*$ character and corresponds to a $\pi_{(Th-N)} \rightarrow \pi^*_{(Th-N)}$ excitation at ~33 000 cm^{-1}. The next two transitions involve the vacant $\pi^*_{(Ph)}$ manifold localized on the hydrazonato ligands as acceptor orbitals [$\pi_{(Th-C_5Me_5)} \rightarrow \pi^*_{(Ph)}$ (36 000 cm^{-1}) and $\pi_{(Th-N)} \rightarrow \pi^*_{(Ph)}$ (38 000 cm^{-1})]. Finally, the LMCT transition $\pi_{(Th-C_5Me_5)} \rightarrow 5f_{(Th)}$ is anticipated to occur at higher energy (38 000 cm^{-1}). For the uranium complex **14**, the same transitions as for **15** are expected, with the $\pi \rightarrow \pi^*$ transitions [$\pi_{(U-C_5Me_5)} \rightarrow \pi^*_{(U-N)}$ (31 000 cm^{-1}) and $\pi_{(U-N)} \rightarrow \pi^*_{(U-N)}$ (33 000 cm^{-1})] being observed at lower energy than the $\pi \rightarrow \pi^*$ transitions involving the $\pi^*_{(Ph)}$ vacant orbitals [$\pi_{(U-C_5Me_5)} \rightarrow \pi^*_{(Ph)}$ (36 000 cm^{-1}) and $\pi_{(U-N)} \rightarrow \pi^*_{(Ph)}$ (38 000 cm^{-1})]. However, the presence of the two occupied uranium 5f orbitals within the seven orbitals of the 5f manifold provides additional absorption bands. While the energies of the f−f excitations in the near-IR region cannot be estimated adequately using simple orbital-energy differences, the calculated energy gaps do represent approximate values for the LMCT

(51) A similar population analysis has been conducted on **Zr-IIb**. This complex bears a charge of +1.68 and presents the following configuration: $(5s,5p)^{0.15}(6d)^{2.17}$. The participation of the metal is 12.4% in the Zr−NCH$_3$ amide σ bonds (with 97.1% d character) and 8.8% in the dative Zr−NCH$_2$ σ bonds (with 84.7% d character).

(52) Clark, A. E.; Martin, R. L.; Hay, P. J.; Green, J. C.; Jantunen, K. C.; Kiplinger, J. L. *J. Phys. Chem. A* **2005**, *109*, 5481–5491.

(53) In the experimental systems, the $\pi_{(An-N)}$ orbitals are found to be slightly below the $\pi_{(An-C_5Me_5)}$ MOs. This small difference with the model compounds **An-IIb** is due to the presence of the phenyl rings in the real systems that stabilize the nitrogen π lone pairs.

Scheme 4. Energy Profile for the Migratory Insertion of H$_2$CN$_2$ into the M−C Bond of the Mono(hydrazonato) Species **M-Ia** To Give the Bis(hydrazonato) Complexes **M-IIa** (M = Zr, Th)
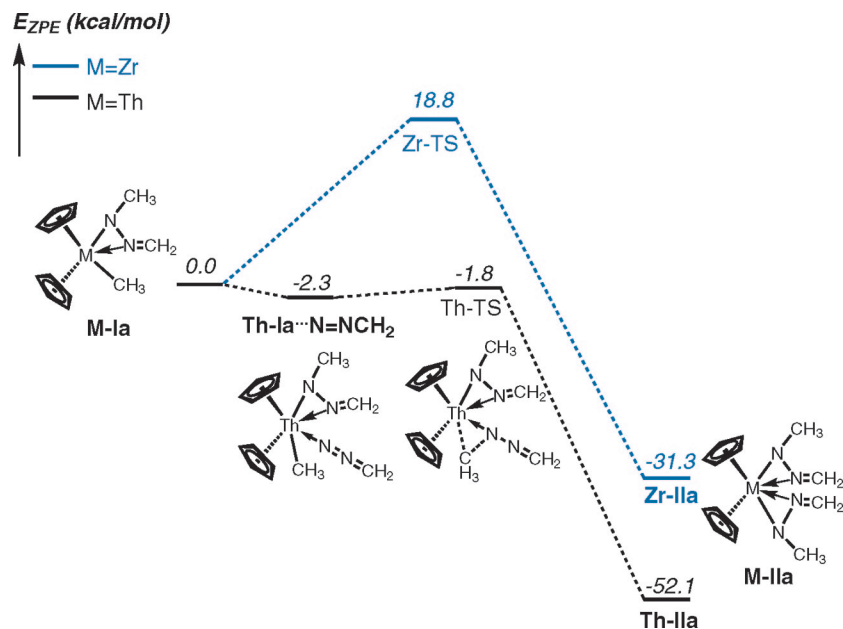
transitions [$\pi_{(U-C_5Me_5)} \rightarrow 5f_{(U)}$ at 26 000 cm^{-1} and $\pi_{(U-N)} \rightarrow 5f_{(U)}$ at 27 000−34 000 cm^{-1}] and the MLCT transitions [$5f_{(U)} \rightarrow \pi^*_{(U-N)}$ at 29 000 cm^{-1} and $5f_{(U)} \rightarrow \pi^*_{(Ph)}$ at 34 000 cm^{-1}].

2.3. Reactivity. To gain insight into why transition metals and actinides react differently, the thermodynamic and kinetic factors for the diazoalkane migratory insertion chemistry were examined. As mentioned above, the reaction between (C$_5$H$_5$)$_2$Zr(CH$_3$)$_2$ and diazoalkanes has been explored experimentally,[27,28] and subsequent theoretical studies of the reaction pathway showed that the three isomers **a**−**c** give the same profiles.[43] It has been demonstrated that the first insertion of one molecule of diphenyl-diazomethane into one Zr−CH$_3$ bond to form the mono(hydra-zonato) complex (C$_5$H$_5$)$_2$Zr[η^2-(N,N')-CH$_3$−N−N=CPh$_2$](CH$_3$) is a low-energy process. The second insertion, which would lead to the bis(hydrazonato) complex, is experimentally unfeasible even under forcing conditions, whereas both insertions are easy processes for actinides (Th and U) and readily occur at ambient temperature. In view of these results, we examined only the second migratory insertion. The reference point was [**M-Ia** + H$_2$CN$_2$], which is the starting point for the migratory insertion of H$_2$CN$_2$ into the M−C bond of the mono(hydrazonato) species **M-Ia** to give the bis(hy-drazonato) products **M-IIa** (Scheme 4).[54] The present results include zero-point energy (ZPE) corrections but do not incorporate solvent effects.

From a thermodynamic standpoint, the reaction is highly exothermic for all of the complexes (Scheme 4 and Figure 3), as expected because of the formation of M−N and C−N bonds. The thermodynamic stability of the putative zirconium bis(hy-drazonato) complex **Zr-IIa** ($\Delta E = -31.3$ kcal/mol) shows that a simple steric difference due to the smaller ionic radius of Zr^{IV} [r(Zr^{IV}) = 0.89 Å, r(Th^{IV}) = 1.09 Å, r(U^{IV}) = 1.05 Å][41] is not responsible for preventing the formation of this complex. In fact, the argument that steric factors govern the difference in reactivity between zirconium and the actinides in this transfor-mation can be completely ruled out, since complexes which are

more sterically congested than the putative **Zr-IIa** complex have already been reported for zirconium. For example, the aminal complexes (C$_5$R$_5$)$_2$Zr[η^4-(C,N,N',C')-CH$_2$N(R')CH$_2$N(R')CH$_2$] (R = H, Me; R' = Me, ^{i}Pr) have been isolated, even in the presence of the sterically demanding C$_5$Me$_5$ ligand.[55] Additionally, (C$_5$H$_5$)$_2$Zr[η^4-(N,N',N'',N''')-{EtO$_2$C(H)C}=N−N−(PPh)$_3$−N−N={C(H)CO$_2$Et}] was obtained successfully by the double insertion of ethyl diazoacetate into both Zr−P bonds of (C$_5$H$_5$)$_2$Zr[η^2-(P,P')-(PPh−PPh−PPh)].[56,57] The calculations for the formation of **U-IIa** from **U-Ia** indicate that replacing one U−CH$_3$ bond with one U−N$_{amide}$ and one U−N$_{dative}$ bond is worth 48 kcal/mol. A similar energy is computed for the formation of **Th-IIa** from **Th-Ia**, suggesting rather compa-rable values for Th−N and U−N bond energies in comparison with Th−C and U−C bonds. Comparison with the Zr system is very informative. Addition of H$_2$CN$_2$ to **Zr-Ia** releases only 31.3 kcal/mol, indicating that the ability of the actinide bent-metallocene fragment (C$_5$H$_5$)$_2$An (An = Th, U) to accom-modate four ligands in its equatorial wedge (vs three for a d-block metallocene) results in an energy difference of ~20 kcal/mol between the corresponding transition-metal and actinide **M-IIa**−**c** complexes. In view of the results obtained regarding the electronic structure of the bis(hydrazonato) complexes (**M-IIa**−**c**), this difference is attributed to a larger ionic radius of the metal ion *and* to the involvement of 5f orbitals in stabilizing the ligand σ and π systems. Neverthe-less, the addition of H$_2$CN$_2$ to **Zr-Ia** remains exothermic enough to suggest that this process is thermodynamically favorable overall and that the experimental difference between the transition-metal and actinide systems for this reaction arises from kinetic rather than thermodynamic considerations.

(54) We have limited our investigation to the **a** isomers, as the same profiles could be reasonably admitted for isomers **b** and **c**. This has been verified previously in the case of Zr (see ref 43).

(55) Karsch, H. H.; Schreiber, K. A.; Reisky, M. *Organometallics* **1998**, *17*, 5052−5060.
(56) The higher reactivity of (C$_5$H$_5$)$_2$Zr[η^2-(P,P')-(PPh−PPh−PPh)] than (C$_5$H$_5$)$_2$Zr(CH$_3$)$_2$ toward diazoalkanes can be attributed to the Zr−P bonds, which are weaker and more polarizable than Zr−C bonds.
(57) Hey, E.; Weller, F. *Chem. Ber./Recl.* **1988**, *121*, 1207−1211.

Earlier studies on the conversion of **Zr-Ia** to **Zr-IIa** calculated a bimolecular transition state (**Zr-TS**) at +18.8 kcal/mol (Scheme 4).[43] For thorium, the addition of H_2CN_2 to **Th-Ia** forms the stable diazoalkane adduct **Th-Ia···N=NCH₂** with an energy slightly below that of the starting materials. The formation of this adduct is in complete agreement with the ability of the $(C_5H_5)_2$Th fragment to accommodate a fourth ligand in its girdle. According to the NBO analysis of the diazoalkane adduct **Th-Ia···N=NCH₂**, the Th←N=NCH₂ bonding interaction consists of the donation of the nitrogen lone pair (93.1%) to a metal hybrid orbital (6.9%) for which the contribution of 5f orbitals is 41.2% and that of 6d is 44.0%. Thus, the Th←N=NCH₂ bond involves significant 5f orbital participation and is essentially equivalent to the Th—N bonds in the final complex **Th-IIa**. In contrast, a similar adduct for the Zr system could not be located. Conversion of the adduct **Th-Ia···N=NCH₂** to **Th-IIa** is straightforward and occurs through an early transition state (**Th-TS**) with a very low energy barrier (0.5 kcal/mol). The same energy profile was computed for thorium with the more bulky C_5Me_5 ligand to verify that using the C_5H_5 ligand in the model complexes did not affect the conclusions. In an analogous manner to the C_5H_5 system, the addition of $H_2C=N_2$ to $(C_5Me_5)_2$Th[η^2-(*N,N'*)-CH_3—N—N=CH_2](CH_3) leads to an adduct that lies 3.0 kcal/mol above the starting materials (Scheme S1 in the Supporting Information).[58] This adduct proceeds to the final bis(hydrazonato) complex $(C_5Me_5)_2$Th[η^2-(*N,N'*)-CH_3—N—N=CH_2]$_2$ ($\Delta E = -47.4$ kcal/mol) through a transition state with an activation barrier of 1.7 kcal/mol.[58,59] On the whole, replacement of the C_5H_5 ligand by the more realistic C_5Me_5 counterpart only leads to a gross shift in energy of about +5 kcal/mol for the intermediate, transition state, and final product. Importantly, the overall energy demand for this process still remains far below that required for zirconium. According to this reaction profile, the difference in kinetics between actinides and transition metals in their reaction with diazoalkanes is now evident (Scheme 4). Whereas the diazoalkane inserts with almost no energy barrier into the Th—C bond in **Th-Ia**, the same reaction requires ∼19 kcal/mol for the analogous zirconium complex **Zr-Ia**. This marked difference arises from the ability of the actinide to coordinate the diazoalkane using 5f orbitals to form an adduct and participate in the migratory insertion. Indeed, the stabilization of a fourth ligand in the wedge of a metallocene is greater by 20 kcal/mol for actinides compared to transition metals. In the case of Zr, the additional 20 kcal/mol must be overcome *before* the migratory insertion can occur, preventing the formation of the bis(hydrazonato) complex **Zr-IIa**, as observed experimentally.

The scenario for uranium is similar to that for thorium, although a stable adduct analogous to **Th-Ia···N=NCH₂** could not be located on the potential energy surface. Importantly, however, during the geometry optimization process for **U-Ia···N=NCH₂**, a separation of the U←N=NCH₂ interaction was not observed; instead, the direct migratory insertion occurred.[60–62] This is in marked contrast to the zirconium system and strongly suggests that the transformation for uranium

involves the same profile as for thorium but with an even lower energy barrier.

3. Electronic Structure: Comparison of Experiment and Theory. Cyclic voltammetric data have previously been reported in detail for a series of mono- and bis(hydrazonato) complexes of $(C_5Me_5)_2An^{IV}$ (An = Th, U), including **14** and **15**.[63] While there are some minor variations in the redox potentials for the analogous electrochemical processes in these systems, the general behavior is consistent over the entire series of hydrazonato complexes. Here we briefly recap these results to establish the orbital dispositions and relative energies of the highest-energy occupied orbitals (from which electrons are extracted in oxidation) and lowest-energy virtual orbitals (to which electrons are added in reduction) in order to assist in the interpretation of the electronic spectroscopic data. The distinguishing features in the voltammograms of the U^{IV} hydrazonato complexes (including **14**) are a metal-based U^V/U^{IV} oxidation wave at about −0.6 V (all potentials vs $[(C_5H_5)_2Fe]^{+/0}$ in 0.1 M $[Bu_4N][B(C_6F_5)_4]$/THF) and a metal-based U^{IV}/U^{III} reduction wave at about −2.7 V. No metal-based electrochemical processes are observed for the Th^{IV} complexes. Both the Th^{IV} and U^{IV} complexes also exhibit quasi-reversible to irreversible ligand-based redox processes at comparable potentials. Specifically, there is a quasi-reversible hydrazonato-based reduction wave that occurs at ∼3.0 V and an irreversible oxidation wave at ∼1.0 V. This latter process has been observed in nearly every $(C_5Me_5)_2An^{IV}L_2$ (An = Th, U) complex we have investigated, including dihalides and bis(alkyls), suggesting that this oxidation is localized principally on the $C_5Me_5^-$ ligands.[63] It should be noted that the orbital dispositions and relative energies for all of these redox processes are consistent with the MO descriptions and relative energies obtained from the DFT calculations for **14** and **15**, as described above. The accessibility and partial occupancy of the metal-based 5f orbitals in the U^{IV} complexes sets the stage for electronic transitions in these complexes that are not available in the Th^{IV} congeners.

The UV−visible electronic absorption spectra for **14** and **15** in toluene solution are illustrated in Figure 7. It is important to note that complex **14** also exhibits a number of f−f electronic bands in the near-IR region (not illustrated in Figure 7) that derive from the $5f^2$ intraconfiguration transitions.[63] The most important difference between these spectroscopic data for **14** and **15** is the occurrence of the new band(s) that constitute the low-energy tail of the spectral envelope for **14**. This low-energy tail appears to consist of at least two discrete bands (∼21 000 and 24 000 cm^{-1}) having substantially smaller extinction coefficients than the other bands. These bands, which are unique to the U^{IV} system, are assigned to transitions involving the 5f orbital manifold. The DFT calculations described above pertaining to the energies of the occupied and virtual orbitals suggest that transitions unique to the U^{IV} system involving the occupied and virtual 5f orbitals should exist and that these should be the lowest-energy transitions observed in the visible region. Neither the resolution of the spectral data nor the precision of the calculations enables a unique assignment of these low-energy bands for **14**. However, the small apparent extinction coefficients of these bands are consistent with a metal−ligand charge-

(58) See the Supporting Information for further details.

(59) The optimized structure for this transition state presents two imaginary frequencies: the one with greater magnitude (−210.3 cm^{-1}) corresponds to the expected diazoalkane insertion, and the residual imaginary frequency of −29.4 cm^{-1} corresponds to the low-energy rotation of one of the methyl groups of a C_5Me_5 ligand. Attempts to further optimize this saddle point were unsuccessful.
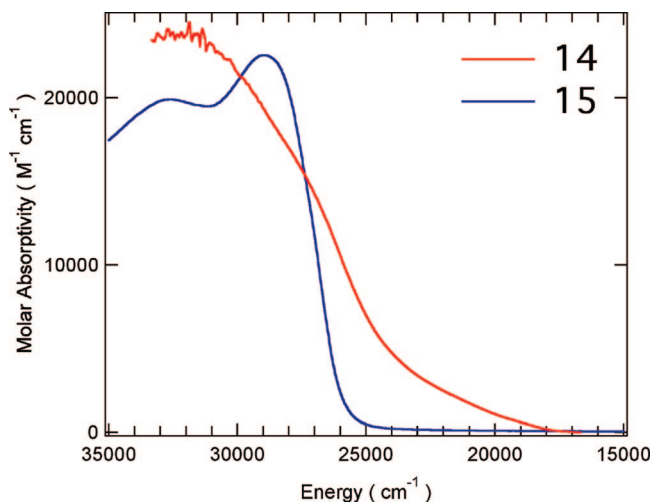
(60) The higher reactivity of uranium compared with thorium has previously been observed: see refs 61 and 62 for examples.

(61) Fagan, P. J.; Manriquez, J. M.; Maatta, E. A.; Seyam, A. M.; Marks, T. J. *J. Am. Chem. Soc.* **1981**, *103*, 6650−6667.

(62) Pool, J. A.; Scott, B. L.; Kiplinger, J. L. *J. Alloys Compd.* **2006**, *418*, 178−183.

(63) Morris, D. E.; Da Re, R. E.; Jantunen, K. C.; Castro-Rodriguez, I.; Kiplinger, J. L. *Organometallics* **2004**, *23*, 5142−5153.

Figure 7. Electronic absorption spectra of $(C_5Me_5)_2An[\eta^2-(N,N')$-$PhCH_2-N-N=CPh_2]_2$ [An = U (**14**), Th (**15**)] in toluene solution.

transfer assignment for which the participating metal orbitals are principally 5f in character, since the charge-transfer intensity scales roughly with the extent of overlap of the metal and ligand orbitals involved in the transition(s).[20,63] The calculations indicate that the lowest-energy one of these charge-transfer bands should have ligand(π)-to-metal(5f) character and that the predicted energies of 26 000–27 000 cm^{-1} for these transitions (obtained using simple orbital-energy differences that ignore exchange and correlation energy contributions) are only slightly greater than the energies of the observed low-energy band(s). This 5f-orbital-derived charge-transfer assignment is also consistent with expectations based on the electrochemical data, since both U^{IV}-based redox couples (oxidation to U^V and reduction to U^{III}) lie between the potentials for ligand-based oxidation and reduction waves.

The DFT calculations suggest that the higher-energy region of the spectra for both **14** and **15** should be similar and comprise ligand-based transitions having $\pi \rightarrow \pi*$ character. The spectrum for **15** (Figure 7) is clearly composed of a series of bands with moderate to high extinction coefficients, consistent with this assignment. The energies of these bands are also in reasonable agreement with those predicted using the orbital-energy differences described above (i.e., 31 000–38 000 cm^{-1}). The apparent differences between **14** and **15** in this higher-energy spectral region are attributable to contributions to the spectral envelope of **14** from additional charge-transfer transitions having metal(5f)-to-ligand($\pi*$) character, as suggested by the DFT calculations. These additional band(s) broaden the spectral envelope, rendering individual $\pi \rightarrow \pi*$ bands (as seen in the spectrum of **15**) unresolved.

Conclusions

In summary, the first bis(hydrazonato) complexes $(C_5Me_5)_2An[\eta^2-(N,N')$-R$-N-N=CPh_2]_2$ have been isolated from the reaction between $(C_5Me_5)_2AnR_2$ (An = Th, U; R = alkyl, aryl) and diphenyldiazomethane. The complexes have been characterized by a combination of NMR and UV–vis–near-IR spectroscopies, elemental analysis, mass spectrometry, cyclic voltammetry, and single-crystal X-ray diffraction.

These actinide complexes have no transition-metal analogues, and the reactions of $(C_5H_5)_2Zr(CH_3)_2$ and $(C_5Me_5)_2Hf(CH_3)_2$ with diphenyldiazomethane give only the corresponding mono(hydra-

zonato) complexes $(C_5R_5)_2M[\eta^2-(N,N')$-CH$_3-N-N=CPh_2](CH_3)$ (M = Zr, R = H; M = Hf, R = CH$_3$). Theoretical calculations afford a model for the structure and reactivity of these complexes that is fully supported by the experimental data. It shows that a significant factor in stabilizing the actinide bis(hydrazonato) complexes is the involvement of 5f orbitals that permits the coordination of four ligands in the equatorial wedge of the metallocene and the stabilization of the occupied π orbitals of the η^2-hydrazonato ligands. This is not available for transition metals, resulting in an energy difference of ~20 kcal/mol between the two series.

The difference in reactivity between the actinide (Th, U) and transition-metal (Zr, Hf) systems was found to stem from kinetic rather than thermodynamic origins, with the actinides being able to use 5f orbitals to facilitate the approach of the diphenyldiazomethane and its insertion into the metal–carbon bond. The insertion of diazoalkane into the actinide–carbon bonds requires a very low energy barrier on the potential energy surface, whereas the barrier reaches ~19 kcal/mol for zirconium. For the thorium system, the reaction profile was computed for both the C$_5$H$_5$ and C$_5$Me$_5$ sets of ligands; the C$_5$Me$_5$ system simply differs from the C$_5$H$_5$ model by a shift of about +5 kcal/mol in the relative energies of the transition state and products. This study also provides clear evidence that thorium(IV) and group 4 metal complexes exhibit significant differences in reactivity and that the generalization that thorium(IV) is merely a large group 4 metal is incorrect. More generally, the presence of 5f orbitals in the valence shell of the actinides that are available for covalent bonding was shown to promote new reactivity patterns by lowering the energies of transition states and intermediates along the reaction pathway.

Experimental Section

Computational Methods. The B3LYP hybrid density functional was employed to optimize the equilibrium molecular structures of the model complexes. The Stuttgart RSC 1997 effective core potential, which incorporates scalar relativistic effects and replaces 60 core electrons, was employed for thorium and uranium. The valence electrons are represented as [8s/7p/6d/4f]; 6-31G* basis sets were used for carbon, hydrogen, and nitrogen. Harmonic vibrational analyses were performed to confirm that structures were minima or saddle points. All of the calculations were carried out using the *Gaussian03* suite of codes.[64]

Instrumentation and Sample Protocols. Electronic absorption spectral data were obtained for a toluene solution of **15** over the wavelength range 280–860 nm on a PerkinElmer model Lambda 950 UV–vis–near-IR spectrophotometer. Data were collected using a 1 mm path length cuvette loaded in the Vacuum Atmospheres drybox system described below and run versus a toluene reference. The spectral resolution was 2 nm. Electronic absorption data were analyzed using Wavemetrics IGOR Pro software (version 6.0) on a Macintosh platform.

General Synthetic Considerations. Unless otherwise noted, all of the reactions and manipulations were performed at 20 °C in a recirculating Vacuum Atmospheres Model HE-553-2 inert atmosphere (N$_2$ or He) drybox with a MO-40-2 Dri-Train or using standard Schlenk techniques. Glassware was dried overnight at 150 °C before use. All of the NMR spectra were obtained using either a Varian Unity Inova or a Bruker Avance 300 MHz spectrometer. Chemical shifts for ^{1}H and ^{13}C{^{1}H} NMR spectra were referenced to solvent impurities. Melting points were determined with a Mel-Temp II capillary melting point apparatus equipped with a Fluke 50S K/J thermocouple using capillary tubes flame-sealed under

(64) Frisch, M. J.; et al. *Gaussian 03*; Gaussian, Inc.: Wallingford, CT, 2004.

nitrogen; values are uncorrected. Mass spectrometric (MS) analyses were obtained at the University of California, Berkeley, mass spectrometry facility using either a VG ProSpec (EI) or a VG70-SE (FAB) mass spectrometer. Elemental analyses were performed at the University of California, Berkeley, Microanalytical Facility on a PerkinElmer Series II 2400 CHNS analyzer.

Unless otherwise noted, reagents were purchased from commercial suppliers and used without further purification. Celite (Aldrich), alumina (Brockman I, Aldrich), and 4 Å molecular sieves (Aldrich) were dried under dynamic vacuum at 250 °C for 48 h prior to use. All of the solvents were purchased anhydrous (Aldrich) and dried over KH for 24 h, passed through a column of activated alumina, and stored over activated 4 Å molecular sieves prior to use. Benzene-d_6 (Aldrich), toluene-d_8 (Aldrich), and tetrahydrofuran-d_8 (THF-d_8) (Cambridge Isotope Laboratories) were purified by storage over activated 4 Å molecular sieves or sodium metal prior to use. $(C_5Me_5)_2Th(CH_3)_2$ (13),[61] $(C_5Me_5)_2Th(CH_2Ph)_2$ (10),[61] $(C_5Me_5)_2Th(Ph)_2$ (11),[65] $(C_5Me_5)_2U(CH_3)_2$ (12),[61] $(C_5Me_5)_2U(CH_2Ph)_2$ (9),[61] $(C_5Me_5)MgCl \cdot THF$,[61] $(C_5Me_5)_2Hf(CH_3)_2$,[66] Ph_2CN_2,[67] and $ThBr_4(THF)_4$[68] were prepared according to literature procedures.

Caution! *Depleted uranium (primary isotope ^{238}U) and natural thorium (primary isotope ^{232}Th) are both weak α-emitters (4.197 and 4.012 MeV, respectively) with a half-lives of 4.47×10^9 and 1.41×10^{10} years, respectively; manipulations and reactions should be carried out in monitored fume hoods or an inert-atmosphere drybox in a radiation laboratory equipped with α- and β-counting equipment.*

Synthesis of $(C_5Me_5)_2ThBr_2$. In a drybox, a 500-mL Schlenk flask equipped with a stir bar was charged with $ThBr_4(THF)_4$ (12.90 g, 15.35 mmol), $(C_5Me_5)MgCl \cdot THF$ (9.02 g, 33.77 mmol), and toluene (300 mL). The reaction vessel was sealed and removed from the drybox to a Schlenk line, where it was placed under a N_2 atmosphere. The reaction mixture was heated to 95 °C with stirring for 15 h and then cooled to room temperature and returned to the drybox. The reaction mixture was transferred to an Erlenmeyer flask, heated to 50 °C, and filtered through a Celite-padded coarse-porosity frit. The filtrate was collected, and the volatiles were removed under reduced pressure. The solid was taken up in a minimal amount of diethyl ether (20 mL), and the resulting slurry was filtered through a fine-porosity frit to give $(C_5Me_5)_2ThBr_2$ as a white solid (9.16 g, 13.83 mmol, 90%). ^{1}H NMR (benzene-d_6, 298 K): δ 2.04 (C_5Me_5).[69]

Synthesis of $(C_5Me_5)_2Hf[\eta^2-(N,N')-CH_3-N-N=CPh_2](CH_3)$. A 50-mL sidearm flask equipped with a stir bar was charged with $(C_5Me_5)_2Hf(CH_3)_2$ (0.479 g, 1.00 mmol) and toluene (10 mL). To the resulting solution was added a toluene (10 mL) solution of diphenyldiazomethane (0.214 g, 1.10 mmol) with stirring. The resultant reaction mixture was stirred at room temperature for 6 days. The volatiles were removed under reduced pressure to afford a pale-pink solid. This solid was washed with cold (−35 °C) pentane (2 × 5 mL) and dried under reduced pressure to afford $(C_5Me_5)_2Hf[\eta^2-(N,N')-CH_3-N-N=CPh_2](CH_3)$ as a white, analytically pure solid (0.542 g, 0.805 mmol, 80%). X-ray-quality crystals were obtained by cooling a solution of the complex in Et$_2$O to −35 °C. ^{1}H NMR (benzene-d_6, 298 K): δ 7.06−7.57 (m, 10H, Ar−*H*), 2.58 (s, 3H, N−C*H*$_3$), 1.86 (s, 30H, C$_5$*Me*$_5$), −0.13 (s, 3H, Hf−C*H*$_3$). ^{13}C{^{1}H} NMR (C$_6$D$_6$, 298 K): δ 139.48, 138.94, 131.69, 127.08, 127.08, 125.63 (Ar−*C*), 115.59 (s, *C*$_5$Me$_5$), 35.75 (s, N−*C*H$_3$), 30.15 (s, Hf−*C*H$_3$), 11.70 (s, C$_5$(*C*H$_3$)$_5$). Anal. Calcd for C$_{35}$H$_{46}$N$_2$Hf (673.24 g/mol): C, 62.44; H, 6.89; N, 4.16. Found: C, 62.61; H, 7.26; N, 3.97.

Note: Attempts to prepare the putative hafnium bis(hydrazonato) complex $(C_5Me_5)_2Hf[\eta^2-(N,N')-CH_3-N-N=CPh_2]_2$ were performed as follows: (i) A solution of $(C_5Me_5)_2Hf(CH_3)_2$ (0.050 g, 0.10 mmol) and diphenyldiazomethane (0.041 g, 0.20 mmol) in toluene-d_8 was heated at 100 °C in a J. Young NMR tube for 18 h. The resulting ^{1}H NMR spectrum indicated the complete formation of the mono(hydrazonato) complex $(C_5Me_5)_2Hf[\eta^2-(N,N')-CH_3-N-N=CPh_2](CH_3)$ and the decomposition of the excess diphenyldiazomethane. (ii) A solution of $(C_5Me_5)_2Hf(CH_3)_2$ (0.050 g, 0.10 mmol) and diphenyldiazomethane (0.078 g, 0.40 mmol) in toluene-d_8 was heated at 80 °C in a J. Young NMR tube for 4 days. The resulting ^{1}H NMR spectrum indicated the complete formation of the mono(hydrazonato) complex $(C_5Me_5)_2Hf[\eta^2-(N,N')-CH_3-N-N=CPh_2](CH_3)$ together with the presence of unreacted diphenyldiazomethane.

Synthesis of $(C_5Me_5)_2U[\eta^2-(N,N')-PhCH_2-N-N=CPh_2]_2$ (14). A 125-mL sidearm flask equipped with a magnetic stir bar was charged with $(C_5Me_5)_2U(CH_2Ph)_2$ (9) (0.354 g, 0.512 mmol) and diethyl ether (60 mL). To the resulting black-green solution was added portion-wise a diethyl ether solution (20 mL) of diphenyldiazomethane (0.253 g, 1.30 mmol) with stirring. The resultant reaction mixture was stirred at room temperature for 8 h, during which time the solution changed color from black-green to dark-cherry-red and crude **14** precipitated from solution. The product was collected by filtration, washed with hexanes (2 × 10 mL), and dried under reduced pressure to afford analytically pure **14** as an orange solid (0.453 g, 0.419 mmol, 82%). ^{1}H NMR (THF-d_8, 323 K): δ 9.23 (t, $J = 7.5$ Hz, 4H, Ar−*H*), 8.99 (t, $J = 7.2$ Hz, 2H, Ar−*H*), 8.77 (br s, 4H, C*H*$_2$C$_6$H$_5$), 7.82 (t, $J = 7.5$ Hz, 2H, CH$_2$C$_6$*H*$_5$ para), 7.45 (t, $J = 7.5$ Hz, 4H, Ar−*H*), 7.19 (t, $J = 6.9$ Hz, 2H, Ar−*H*), 7.11 (t, $J = 6.9$ Hz, 2H, Ar−*H*), 6.64 (t, $J = 7.2$ Hz, 4H, CH$_2$C$_6$*H*$_5$ meta), 6.37 (t, $J = 7.5$ Hz, 2H, Ar−*H*), 4.95 (d, $J = 6.9$ Hz, 4H, CH$_2$C$_6$*H*$_5$ ortho), 4.78 (t, $J = 7.2$ Hz, 4H, Ar−*H*), 2.52 (s, 30H, C$_5$*Me*$_5$). UV−vis−NIR (toluene) λ (nm) (ε, M^{-1} cm^{-1}): 311 (23 400), 440 (3050), 656 (26), 692 (71), 723 (45), 740 (36), 776 (19), 838 (19), 859 (26), 870 (21), 922 (16), 991 (69), 1092 (89), 1137 (80), 1173 (86), 1233 (55), 1294 (50), 1381 (124), 1528 (28). U$^{IV/III}$ $E_{1/2} = -2.56$ V; U$^{V/IV}$ $E_{1/2} = -0.48$ V (vs [(C$_5$H$_5$)$_2$Fe]$^{0/+}$). Mp: 242−244 °C. MS (FAB, Cs 20 kV): m/z 1078.7 [M$^+$], 943.5 [M$^+$ − C$_5$Me$_5$]. Anal. Calcd for C$_{60}$H$_{64}$N$_4$U (1079.21 g/mol): C, 66.78; H, 5.98; N, 5.19. Found: C, 66.45; H, 6.05; N, 5.07.

Synthesis of $(C_5Me_5)_2Th[\eta^2-(N,N')-PhCH_2-N-N=CPh_2]_2$ (15). A 125-mL sidearm flask equipped with a magnetic stir bar was charged with $(C_5Me_5)_2Th(CH_2Ph)_2$ (10) (0.596 g, 0.871 mmol) and diethyl ether (50 mL). To the resulting white slurry was added portion-wise a diethyl ether solution (20 mL) of diphenyldiazomethane (0.389 g, 2.00 mmol) with stirring. The resultant reaction mixture was stirred at room temperature for 4 h, during which time the solution changed color from white to orange and crude **15** precipitated from solution. The product was collected by filtration, washed with hexanes (2 × 10 mL), and dried under reduced pressure to afford **15** as white powder. Analytically pure samples of **15** were obtained by recrystallization from hot toluene (0.490 g, 0.456 mmol, 52%). ^{1}H NMR (THF-d_8, 298 K): δ 7.39−6.44 (m, 30H, Ar−*H*), 5.04 (d, $J = 5$ Hz, 2H, C*H*$_2$Ph), 4.38 (s, 2H, C*H*$_2$Ph), 2.14 (s, 15H, C$_5$*Me*$_5$), 1.92 (s, 15H, C$_5$*Me*$_5$). ^{13}C{^{1}H} NMR (THF-d_8, 298 K): δ 144.61, 142.59, 142.29, 141.61, 140.47, 138.31, 137.80, 136.15, 132.12, 129.00, 128.87, 128.75, 128.36, 128.15, 127.74, 127.54, 127.31, 127.18, 126.84, 126.75, 126.50, 126.26 (Ar−*C*), 125.34 (s, *C*$_5$Me$_5$), 124.49 (s, *C*$_5$Me$_5$), 57.48 (s, *C*H$_2$Ph), 55.48 (s, *C*H$_2$Ph), 12.83 (s, C$_5$(*C*H$_3$)$_5$), 12.39 (s, C$_5$(*C*H$_3$)$_5$). Mp: >230 °C. Anal. Calcd for C$_{60}$H$_{64}$N$_4$Th (1073.22 g/mol): C, 67.15; H, 6.01; N, 5.22. Found: C, 66.82; H, 6.05; N, 5.26.

Synthesis of $(C_5Me_5)_2Th[\eta^2-(N,N')-Ph-N-N=CPh_2]_2$ (16). A 125-mL sidearm flask equipped with a stir bar was charged with $(C_5Me_5)_2ThPh_2$ (11) (0.584 g, 0.889 mmol) and diethyl ether (60 mL). To the resulting solution was added a diethyl ether solution (20 mL) of diphenyldiazomethane (0.380 g, 1.96 mmol) with

(65) England, A. F.; Burns, C. J.; Buchwald, S. L. *Organometallics* **1994**, *13*, 3491–3495.
(66) Schock, L. E.; Marks, T. J. *J. Am. Chem. Soc.* **1988**, *110*, 7701–7715.
(67) Miller, J. B. *J. Org. Chem.* **1959**, *24*, 560–561.
(68) Clark, D. L.; Frankcom, T. M.; Miller, M. M.; Watkin, J. G. *Inorg. Chem.* **1992**, *31*, 1628–1633.
(69) Rabinovich, D.; Bott, S. G.; Nielsen, J. B.; Abney, K. D. *Inorg. Chim. Acta* **1998**, *274*, 232–235.

stirring. The resultant reaction mixture was stirred at room temperature for 15 h, during which time the solution changed from colorless to dark-red and a white solid precipitated from solution. The solid was collected by filtration, washed with hexanes (2 × 10 mL), and dried under reduced pressure to afford crude **16** as a pale-yellow solid. Analytically pure samples of **16** were obtained by recrystallization from toluene at −30 °C (0.522 g, 0.499 mmol, 56%). ^{1}H NMR (THF-d_8, 298 K): δ 7.50 (d, J = 7.5 Hz, 4H, Ar−*H*), 7.29−7.13 (m, 12H, Ar−*H*), 6.98 (m, 4H, Ar−*H*), 6.88 (m, 3H, Ar−*H*), 6.75 (m, 3H, Ar−*H*), 6.65 (m, 2H, Ar−*H*), 6.59 (m, 2H, Ar−*H*), 1.78 (s, 30H, C$_5$M*e*$_5$). ^{13}C{^{1}H} NMR (THF-d_8, 298 K): δ 150.20, 144.72, 139.68, 138.55, 129.50, 128.85, 128.52, 128.18, 127.95, 127.70, 127.31, 126.52 (Ar-*C*), 124.72 (s, *C*$_5$Me$_5$), 124.39 (Ar-*C*), 12.36 (s, C$_5$(*C*H$_3$)$_5$). Mp: >230 °C. Anal. Calcd. for C$_{58}$H$_{60}$N$_4$Th (1045.16 g/mol): C, 66.65; H, 5.79; N, 5.36. Found: C, 66.85; H, 5.95; N, 5.24.

Synthesis of (C$_5$Me$_5$)$_2$U[η^2-(*N*,*N*′)-CH$_3$−N−N=CPh$_2$]$_2$ (17). A 125-mL sidearm flask equipped with a stir bar was charged with (C$_5$Me$_5$)$_2$U(CH$_3$)$_2$ (**11**) (0.595 g, 1.11 mmol) and diethyl ether (60 mL). To the resulting orange solution was added portion-wise a diethyl ether solution (20 mL) of diphenyldiazomethane (0.500 g, 2.57 mmol) with stirring to give an exothermic reaction. The resultant reaction mixture was stirred at room temperature for 12 h, during which time the solution changed color from orange to dark-cherry-red. The reaction mixture was then filtered through a Celite-padded coarse frit and the filtrate collected, after which the volatiles were removed under reduced pressure to afford a dark-red solid. This solid was taken up in a minimal amount of diethyl ether (7 mL), layered with hexanes (10 mL), and stored at −30 °C to give **17** as a dark-red crystalline solid (0.726 g, 0.783 mmol, 71%). ^{1}H NMR (toluene-d_8, 298 K): three distinct C$_5$Me$_5$-containing species were present at δ 2.51, −0.37, and −1.32 in a 2:5:3 ratio at ambient temperature; coalescence was not completely observed upon heating to 110 °C, and cooling back to ambient temperature regenerated the mixture of isomers in the same ratio. UV−vis−NIR (toluene) λ (nm) (ε, M^{-1} cm^{-1}): 316 (25 500), 460 (3060), 675 (65), 688 (66), 712 (49), 744 (35), 845 (27), 907 (43), 992 (73), 1050 (71), 1082 (88), 1133 (82), 1163 (82), 1232 (70), 1360 (70), 1383 (84), 1440 (45), 1519 (37), 1565 (35). U$^{IV/III}$ $E_{1/2}$ = −2.62 V; U$^{V/IV}$ $E_{1/2}$ = −0.51 V (vs [(C$_5$H$_5$)$_2$Fe]$^{0/+}$). Mp: 229−231 °C. MS (EI, 70 eV): m/z 926.6 [M$^+$], 791.3 [M$^+$ − C$_5$Me$_5$]. Anal. Calcd for C$_{48}$H$_{56}$N$_4$U (926.98 g/mol): C, 62.19; H, 6.09; N, 6.04. Found: C, 62.13; H, 6.10; N, 5.96.

Synthesis of (C$_5$Me$_5$)$_2$Th[η^2-(*N*,*N*′)-CH$_3$−N−N=CPh$_2$]$_2$ (18). A 125-mL sidearm flask equipped with a stir bar was charged with (C$_5$Me$_5$)$_2$Th(CH$_3$)$_2$ (**13**) (0.739 g, 1.39 mmol) and diethyl ether (50 mL). To the resulting clear, colorless solution was added portion-wise a diethyl ether solution (20 mL) of diphenyldiazomethane (0.596 g, 3.05 mmol) with stirring. The resultant reaction mixture was stirred at room temperature for 6 h, during which time the solution changed color to dark-red. The reaction mixture was filtered through a Celite-padded coarse frit. The filtrate was collected, and the volatiles were removed under reduced pressure to afford an orange solid. The crude product was collected by filtration using a fine frit, washed with hexanes (2 × 10 mL), and dried under reduced pressure to afford **18** as a white powder. Analytically pure samples of **18** were obtained by recrystallization from hot hexanes (0.807 g, 0.875 mmol, 63%). ^{1}H NMR (benzene-d_6, 298 K): δ 7.68−6.99 (m, 20H, Ar−*H*), 3.13 (s, 3H, −C*H*$_3$), 2.95 (s, 3H, −C*H*$_3$), 2.02 (s, 30H, C$_5$M*e*$_5$). ^{13}C{^{1}H} NMR (benzene-d_6, 298 K): δ 142.94, 140.88, 135.04, 131.82, 128.45, 127.84, 127.56, 127.10, 126.51, 124.18, 123.61, 43.02, 32.30, 23.38, 14.69, 12.35. Mp: 213−215 °C. Anal. Calcd for C$_{48}$H$_{56}$N$_4$Th (921.02 g/mol): C, 62.59; H, 6.13; N, 6.08. Found: C, 62.38; H, 6.39; N, 5.83.

Crystallographic Experimental Details. The crystal structures of compounds **14**, **15**, **17a**, and **18a** and of (C$_5$Me$_5$)$_2$Hf[η^2-(*N*,*N*′)-CH$_3$−N−N=CPh$_2$](CH$_3$) were determined as described below, with exceptions noted in the following paragraphs: Single crystals were mounted in a nylon cryoloop using Paratone-N oil under an argon flow. The data were collected on a Bruker P4/1k-CCD diffractometer with a Bruker LT-2 temperature device. The instrument was equipped with a graphite-monochromatized Mo Kα X-ray source (λ = 0.71073 Å). A hemisphere of data was collected using φ scans with 30 s frame exposures and 0.3° frame widths. Data collection and initial indexing and cell refinement were handled using SMART software.[70] Frame integration, including Lorentz-polarization corrections, and final cell-parameter calculations were carried out using SAINT software.[71] The data were corrected for absorption using the SADABS program.[72] The decay of reflection intensity was monitored by analysis of redundant frames. The structure was solved using direct methods (SHELXS-97) and difference Fourier techniques. All of the non-hydrogen atoms were refined anisotropically, and hydrogen atom positions were treated as idealized contributions. The final refinement included anisotropic temperature factors on all of the non-hydrogen atoms (SHELXL-97). Structure solution, refinement, graphics, and creation of publication materials were performed using SHELXTL version 6.10.[73]

For compound **14**, the crystal contained three domains, all of which were indexed. Attempts to integrate the intensity data using all of the domains were unsuccessful. The integration and refinement were performed with the primary domain, and 297 reflections affected by twinning were omitted in the final refinement.

For compound **15**, one solvent molecule of *n*-hexane per complex was found in the difference map and refined with anisotropic temperature factors and hydrogen atom positions.

For (C$_5$Me$_5$)$_2$Hf[η^2-(*N*,*N*′)-CH$_3$−N−N=CPh$_2$](CH$_3$), the data were collected using a Bruker SMART APEX II CCD diffractometer with a KRYOFLEX liquid nitrogen vapor cooling device. The C$_5$Me$_5^-$ group containing carbon atoms C11−C14(A/B) were well-defined with 1:1 occupancies between two parts, including the respective methyl groups. The atoms were set to idealized positions using FLAT and DFIX cards in the refinement and were refined isotropically. The displacement of the disordered components of C$_5$Me$_5^-$ comprising atoms C1−C5 was found to be smaller, so the atoms of the ring could be modeled using single positions and refined anisotropically without setting idealized positions for these atoms. The elongation of these ring carbon atom thermal ellipsoids is a reflection of the disorder. The methyl groups of these carbon atoms were found to have a larger disordered displacement and were similarly modeled over two positions and refined isotropically. Residual electron density was accounted for using the SQUEEZE refinement.[74]

(70) *SMART-NT*, version 4; Bruker AXS, Inc.: Madison, WI, 1996.
(71) *SAINT-NT*, version 5.050; Bruker AXS, Inc.: Madison, WI, 1998.
(72) Sheldrick, G. M. *SADABS*; University of Göttingen: Göttingen, Germany, 1996.
(73) *SHELXTL NT*, version 6.10; Bruker AXS, Inc.: Madison, WI, 2001.
(74) Spek, A. L. *PLATON: A Multipurpose Crystallographic Tool*; Utrecht University: Utrecht, The Netherlands, 2005.

Supporting Information Available: Crystallographic data for **14**, **15**, **17a**, **18a**, and $(C_5Me_5)_2Hf[\eta^2\text{-}(N,N')\text{-}CH_3-N-N{=}CPh_2]\text{-}(CH_3)$ (PDF, CIF); the full MO diagram for **Th-IIb**, **U-IIb**, and **Zr-IIb**; the reaction profile calculated for the $(C_5Me_5)_2Th[\eta^2\text{-}$ $(N,N')\text{-}CH_3-N-N{=}CH_2](CH_3)$ system; *XYZ* data for **M-Ia−c** and **M-IIa−c** (M = Th, U), **Zr-IIb**, **Th-Ia···N₂=CH₂**, **Th-TS, Th-Ia***, **Th-Ia*···N₂=CH₂**, and **Th-TS***; and complete ref 64. This material is available free of charge via the Internet at http://pubs.acs.org.

JA8067287